1973-04-01

^{7}Li(d,p)^{8}Li excitation function :|bE[subscript d] = 0.623 MeV to 1.968 MeV

Albert E. Schilling
Brigham Young University - Provo

$^{7}Li(d,p)^{8}Li$ EXCITATION FUNCTION: E_d = 0.623MeV TO 1.968MeV

A Thesis

Presented to the

Department of Chemistry

Brigham Young University

In Partial Fulfillment

of the Requirements for the Degree

Master of Science

by

Albert E. Schilling

April 1973

This thesis, by Albert E. Schilling, is accepted in its present form by the Department of Chemistry of Brigham Young University as satisfying the thesis requirement for the degree of Master of Science.

ACKNOWLEDGEMENTS

This author would like to express a sincere thanks to his major professors, Dr. Nolan F. Mangelson, whose advice, patience, and many hours of effort have made this study possible.

Thanks is given to Brigham Young University for the financial support in the form of teaching assistantships and research funds.

Special appreciation is expressed to my wife, Gerrie, for her patience and understanding throughout this study. Appreciation is also given to my parents for their support and encouragement.

Last, but not least, thanks is given to Drs. Dwight Dixon, Max Hill, Coran Cluff, Gary Jensen, Vern Rogers, Paul Steed, Ivan Rezanka and Rolland Perry. A sincere thanks is also given to the following graduate students: Kirk Nielson, Robert Melton, George Allison, John Moellmer, Leon Pahler, Art Cumminings, Bill Johnston, Dennis Hunt and many others too numerous to mention whose continuous friendship has made this study both enjoyable and worthwhile.

TABLE OF CONTENTS

I. INTRODUCTION 1

Statement of Problem
The $^{7}Li(d,p)^{8}Li$ Reaction

II. LITERATURE REVIEW 7

Summary of Literature Review

III. EXPERIMENTAL CONSIDERATIONS 14

General Information
Apparatus and Experimental Arrangement
Procedures Used in Obtaining Data

IV. DATA ANALYSIS AND EXCITATION FUNCTION 23

Data Analysis
$^{7}Li(d,p)^{8}Li$ Excitation Function
Summary of Nuclear Parameters

V. DISCUSSION 40

Target Thickness Effects
Widths in ^{8}Be and ^{9}Be

VI. SUMMARY 46

APPENDIX A 48

APPENDIX B 52

APPENDIX C 53

LIST OF REFERENCES 57

LIST OF TABLES

Table		Page
1.	Calculated Nuclear Parameters for the $^{7}Li(d,p)^{8}Li$ Reaction	4
2.	Half-life Values for the ^{8}Li Beta Decay	12
3.	Cross Section Values at Resonances for the $^{7}Li(d,p)^{8}Li$ Reaction at Deuteron Energies Ranging from 0.25MeV to 1.10MeV	13
4.	Experimental Parameters for the $^{7}Li(d,p)^{8}Li$ Reaction . . .	13
5.	Cross Section and Widths of Resonances for the $^{7}Li(d,p)^{8}Li$ Reaction	38
6.	Measured Nuclear Parameters of the $^{7}Li(d,p)^{8}Li$ Reaction .	38

LIST OF FIGURES

Figure — Page

1. Level Diagram for the $^{7}Li(d,p)^{8}Li(\beta,\nu)^{8}Be(2\alpha)$ Reaction 3

2. Center-of-mass Schematic for an Endoergic Nuclear Reaction 5

3. $^{7}Li(d,p)^{8}Li$ Excitation Functions by Baggett & Bame[5] Kavanagh[9], Bashkin[6], and Bennett[4] et al. 9

4. $^{7}Li(d,p)^{8}Li$ Excitation Functions by Imhof[14] et al. and Woods & Wilkinson[13] 11

5. Physical Arrangement of Cold Trap, Collimators, Faraday Cup, and Target-detector Assembly 16

6. Physical Arrangement of Accelerator and Related Equipment 18

7. Block Diagram of the Electronics for this Study Illustrating Both the Cyclic System and Detection and Counting Systems 19

8. Schematic Illustration of the Timing Sequence for the Cyclic System 21

9. Delayed Alpha Spectrum from the Decay of the 2.90MeV Level of ^{8}Be. This Alpha Spectrum Contains 532,580 Total Alpha Counts. $E_d = 0.689MeV$ 24

10. Delayed Alpha Spectrum from the Decay of the 2.90MeV Level of ^{8}Be. This Alpha Spectrum Contains 602,407 Total Alpha Counts. $E_d = 0.762MeV$ 25

11. Delayed Alpha Spectrum from the Decay of the 2.90MeV Level of ^{8}Be. This Alpha Spectrum Contains 473,398 Total Alpha Counts. $E_d = 0.932MeV$ 26

12. Delayed Alpha Spectrum from the Decay of the 2.90MeV Level of ^{8}Be. This Alpha Spectrum Contains 296,909 Total Alpha Counts. $E_d = 1.274MeV$ 27

13. Delayed Alpha Spectrum from the Decay of the 2.90MeV Level of ^{8}Be. This Alpha Spectrum Contains 437,356 Total Alpha Counts. $E_d = 1.728MeV$ 28

Figure Page

14. Logarithmic Plot of Delayed Alpha Spectrum Showing the Presence of Another Delayed Emitter. Black Dashed Line Indicates the Subtraction of the Impurity Corresponding to a Height of 207 Counts. E_d = 0.689MeV 30

15. Logarithmic Plot of Delayed Alpha Spectrum Showing the Presence of Another Delayed Emitter. Black Dashed Line Indicates the Subtraction of the Impurity Corresponding to a Height of 240 Counts. E_d = 0.762MeV 31

16. Logarithmic Plot of Delayed Alpha Spectrum Showing the Presence of Another Delayed Emitter. Black Dashed Line Indicates the Subtraction of the Impurity Corresponding to a Height of 275 Counts. E_d = 0.932MeV 32

17. Logarithmic Plot of Delayed Alpha Spectrum Showing the Presence of Another Delayed Emitter. Black Dashed Line Indicates the Subtraction of the Impurity Corresponding to a Height of 431 Counts. E_d = 1.728MeV 33

18. Plot of the Ratio (K) of the Number of Counts in Channel 30 to the Average Number of Counts in the Peak Channel Versus the Magnet Current for Sixteen Alpha Spectra. This Plot Indicates that the Height of the Impurity can be Determined Within 1% 34

19. Plot of the Height of the Impurity Versus the k Value (Eq. 6) for Four Impurity Spectra. This Plot Indicates that the k Value can be Determined Within 0.5% 35

20. Excitation Function for the $^7Li(d,p)^8Li$ Reaction at Deuteron Energies Ranging from 0.623MeV to 1.968MeV. This Excitation Function Reveals Resonances at 0.777 ± 0.012MeV and 1.031 ± 0.015MeV 37

21. Excitation Function for the $^7Li(d,p)^8Li$ Reaction. Dashed Line Indicates the Estimated Non-resonance Background for this Reaction. Subtraction of these Two Excitation Functions is Shown in Figure 22 41

22. Plot of the Resonance Excitation Function for the $^7Li(d,p)^8Li$ Reaction 44

Figure Page

23. Logarithmic Plot of the Breit-Wigner Dispersion Equation and the Experimental Resonance Excitation Function. Black Dashed Line Indicates the Breit-Wigner Dispersion Equation; Black Dotted Line Indicates the Resonance Excitation Function Shown in Figure 22 44

24. Derivation of Cross Section Equation 48

25. Plot Showing Least Squares Fit to the 0.837MeV Resonance From the $^{19}F(p,\alpha\gamma)^{16}O$ Reaction, 0.770MeV Resonance From the $^{7}Li(d,p)^{8}Li$ Reaction, 1.882MeV Resonance From the $^{7}Li(p,n)^{7}Be$ Reaction, and 1.02 MeV Resonance From the $^{7}Li(d,p)^{8}Li$ Reaction Respectively 53

I. INTRODUCTION

A fundamental concept in the study of nuclear reactions is the "probability" of a reaction occurring under a given set of experimental conditions. This probability of occurrence is usually expressed as the "effective area" presented by the target nucleus toward the beam of bombarding particles, such that the number of particles incident upon that area is the number observed to produce the reaction in question. For the purpose of this study the "effective area" or cross section can be considered as being proportional to the ratio of the total number of events which are observed to occur to the product of the total integrated number of incident particles and the number of eligible nuclei per unit area of the target perpendicular to the beam. (For the complete mathematical derivation of the cross section equation see Appendix A).

When the cross section of a nuclear reaction is plotted versus the energy of the bombarding particles, the resultant plot is termed an "excitation function". The excitation function of a particular reaction can be a smooth function of energy or can vary sharply with energy exhibiting peaks at specific energies. Nuclear reactions whose excitation functions vary sharply with energy are termed "resonance reactions" and it is this type of nuclear reaction which pertains to this study.

Statement of Problem

It is the purpose of this study to measure the absolute cross section of the $^{7}Li(d,p)^{8}Li$ reaction at the 0.770MeV and 1.02Mev resonances. This was accomplished by counting the number of delayed alpha-particles as a result of the ^{8}Li beta decay. The excitation function for the $^{7}Li(d,p)^{8}Li$ reaction was experimentally determined at deuteron energies ranging from 0.623MeV to 1.968MeV (see Appendix B for the energy calibration used in the determination of this excitation function).

The $^{7}Li(d,p)^{8}Li$ Reaction

The $^{7}Li(d,p)^{8}Li$ resonance reaction is an endoergic nuclear reaction. The decay scheme for the overall reaction is best illustrated by the level diagram for the $^{7}Li(d,p)^{8}Li$ reaction and is shown in Figure 1. The threshold energy (T_a) for this reaction, calculated by non-relativistic kinematics, is adequately expressed as follows:

$$T_a = -Q(M_x+M_a)/M_x \qquad (1)$$

where T_a and M_a are the kinetic energy and mass respectively of the incident particle in the laboratory system and M_x is the mass of the target particle at rest in the laboratory system. Q represents the change in mass energy or Q value for the $^{7}Li(d,p)^{8}Li$ reaction and is defined as:

$$Q = (M_a+M_x)c^2-(M_b+M_y)c^2 \qquad (2)$$

where M_b represents the mass of the light reaction product and M_y represents the mass of the heavy reaction product. The available energy for this reaction is then given by the expression:

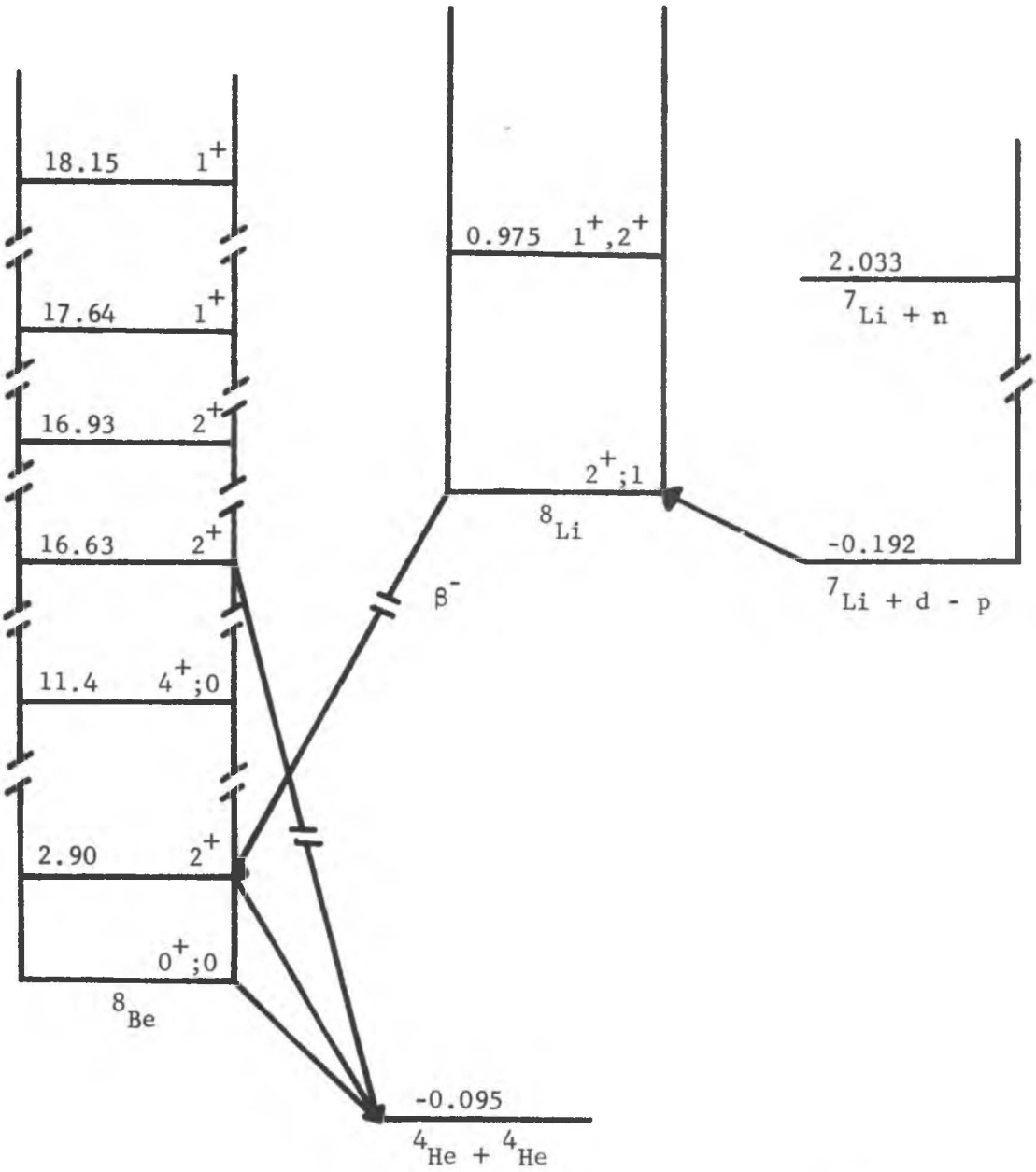

Fig. 1. Level diagram for the $^{7}Li(d,p)^{8}Li(\beta,\nu)^{8}Be(2\alpha)$ reaction.

$$\text{Available Energy} = (Q+T_o) \qquad (3)$$

where T_o is the kinetic energy of the initial particles in the center-of-mass system and is defined as:

$$T_o = M_x T/(M_a+M_x) \qquad (4)$$

where T is the kinetic energy of the incident particle in the laboratory system.

The threshold energy and Q value for the $^{7}Li(d,p)^{8}Li$ reaction, calculated using the atomic mass excess values from Mattauch[1] et al., are listed in Table 1.

TABLE 1

CALCULATED NUCLEAR PARAMETERS FOR THE $^{7}Li(d,p)^{8}Li$ REACTION

Threshold Energy (MeV)	Q Value (MeV)
0.247	-0.192

A simple center-of-mass interpretation showing both the conservation of energy of the system and the formation of an intermediate compound nucleus for an endoergic nuclear reaction can be schematically indicated as in Figure 2. The notation used here is from Meyerhof[2] where $M^*_{(a+x)}$ and M^*_y indicate the total mass energy of the excited compound nucleus and recoil particle respectively. The sequence illustrated in Step A represents an endoergic reaction in which the emergent particles are left in their ground states whereas that sequence given in Step B represents the emergent particles in which M^*_y is left in an excited state.

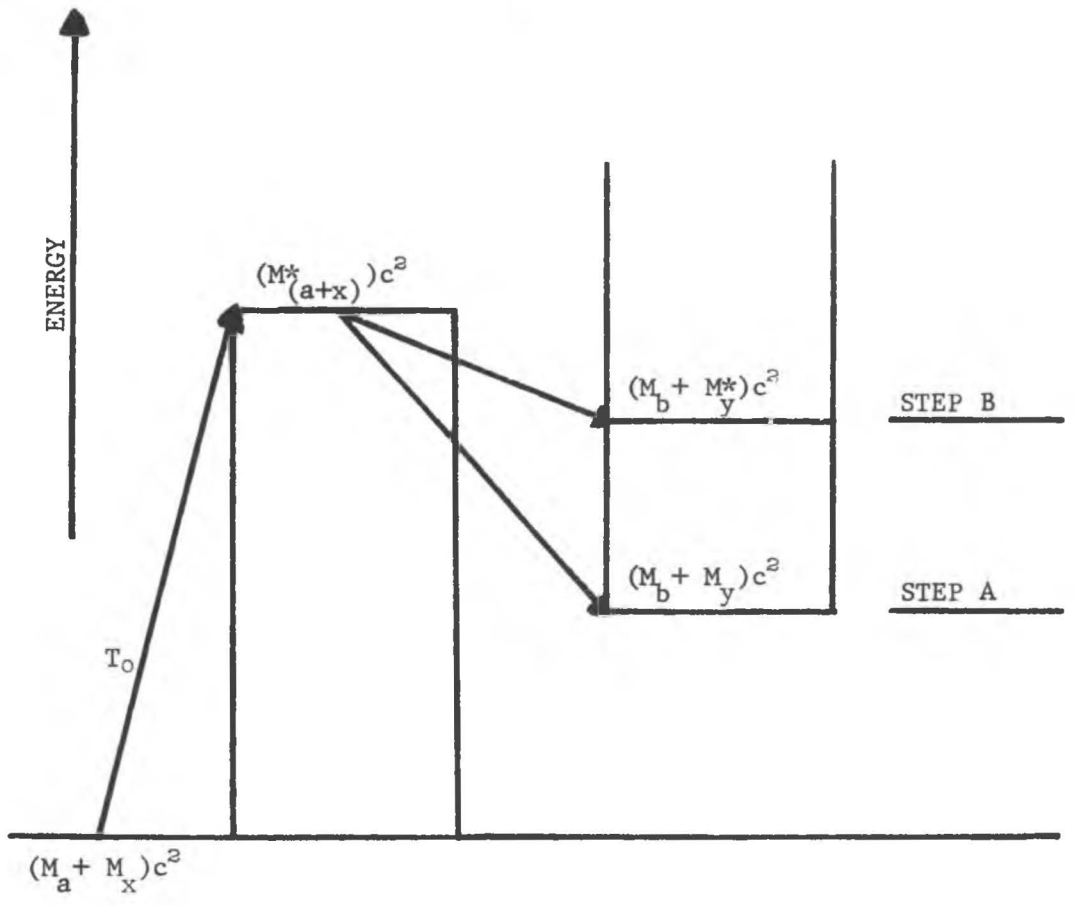

Fig. 2. Center-of-mass schematic for an endoergic nuclear reaction.

The $^{7}Li(d,p)^{8}Li$ reaction is energetically represented as in Step A when M_a and M_x are the masses of the incident deuteron and ^{7}Li atom, respectively. M_b and M_y would then represent the masses of the emergent proton and ^{8}Li recoil atom; and $M^{*}_{(a+x)}$ would represent the excited state of the ^{9}Be compound nucleus.

II. LITERATURE REVIEW

As early as 1938 Rumbaugh[3] et al. measured the yield curve for the production of ^{8}Li from the $^{7}Li(d,p)^{8}Li$ reaction at deuteron energies ranging from 200KeV to 1000KeV. Their results indicated a possible resonance at about 700KeV where a change in slope of the yield curve was observed. These results were later confirmed by Bennett[4] et al. in their investigation of the $^{7}Li(d,p)^{8}Li$ reaction. By counting the beta-particles from the decay of ^{8}Li Bennett et al. observed resonances at 750KeV, 1.02MeV and a possible resonance at 1.35MeV. However, their data did not extend far beyond 1.35MeV; therefore the resonance at 1.35MeV remained in question. The data from Bennett et al. have been arbitrarily plotted in Figure 3 since they show only relative cross sections.

Baggett and Bame[5] measured the excitation function of the $^{7}Li(d,p)^{8}Li$ reaction at deuteron energies up to 1.80MeV by counting the beta-particles released from the decay of ^{8}Li. Their excitation function, also shown in Figure 3, indicates broad resonances at 770KeV and 1.02MeV with a change in slope at 1.40MeV. The target used in this investigation consisted of Li_2SO_4, which being hygroscopic resulted in an uncertainty of 20% in the target weight; therefore, their results are at least uncertain to 20%.

Attempting to clarify the disagreement concerning the resonance at 1.35MeV, Bashkin[6] measured the absolute cross section of the

$^{7}Li(d,p)^{8}Li$ reaction at deuteron energies ranging from 700KeV to 3.30MeV, again by counting the beta-particles from the decay of ^{8}Li. Bashkin's excitation function is also shown in Figure 3 and is consistent with previous data in showing broad resonances at 800KeV and 1.04 MeV. However, despite careful search Bashkin was unable to verify the existence of a resonance at 1.40MeV; instead his data reveals a smooth increase in cross section from 1.20MeV which levels off at about 1.90 MeV. This lack of quantitative agreement between Bashkin's results and the results of Baggett and Bame can be attributed to inadequately corrected background by Baggett and Bame.(6) This background increases steadily as the energy of the incident deuterons is increased, hence the sharp rising curve above 1.40MeV.

Degrading 4.0±0.05MeV deuterons from the 70cm cyclotron at the Academy of Sciences U.S.S.R. through a stack of aluminum foils, Bezrukov[7] et al. determined the excitation function for the $^{7}Li(d,p)^{8}Li$ reaction at deuteron energies ranging from 1.0MeV to 4.0MeV. Their excitation function, determined by counting beta-particles from the decay of ^{8}Li, indicates resonances at 2.0MeV, 2.5MeV and 3.7MeV, but does not reveal a resonance at 1.40MeV.

While studying the competition between compound nucleus formation and stripping in small Q value reactions, J. P. Sellschop[8] measured the angular distribution of protons from the $^{7}Li(d,p)^{8}Li$ reaction at deuteron energies ranging from 0.60MeV to 2.60MeV. Sellschop's data indicates a strong and broad resonance at 1.40MeV and stands in disagreement with measurements of the beta yield for this same reaction by other researchers.[6,7,9]

In the process of measuring the absolute cross section of the

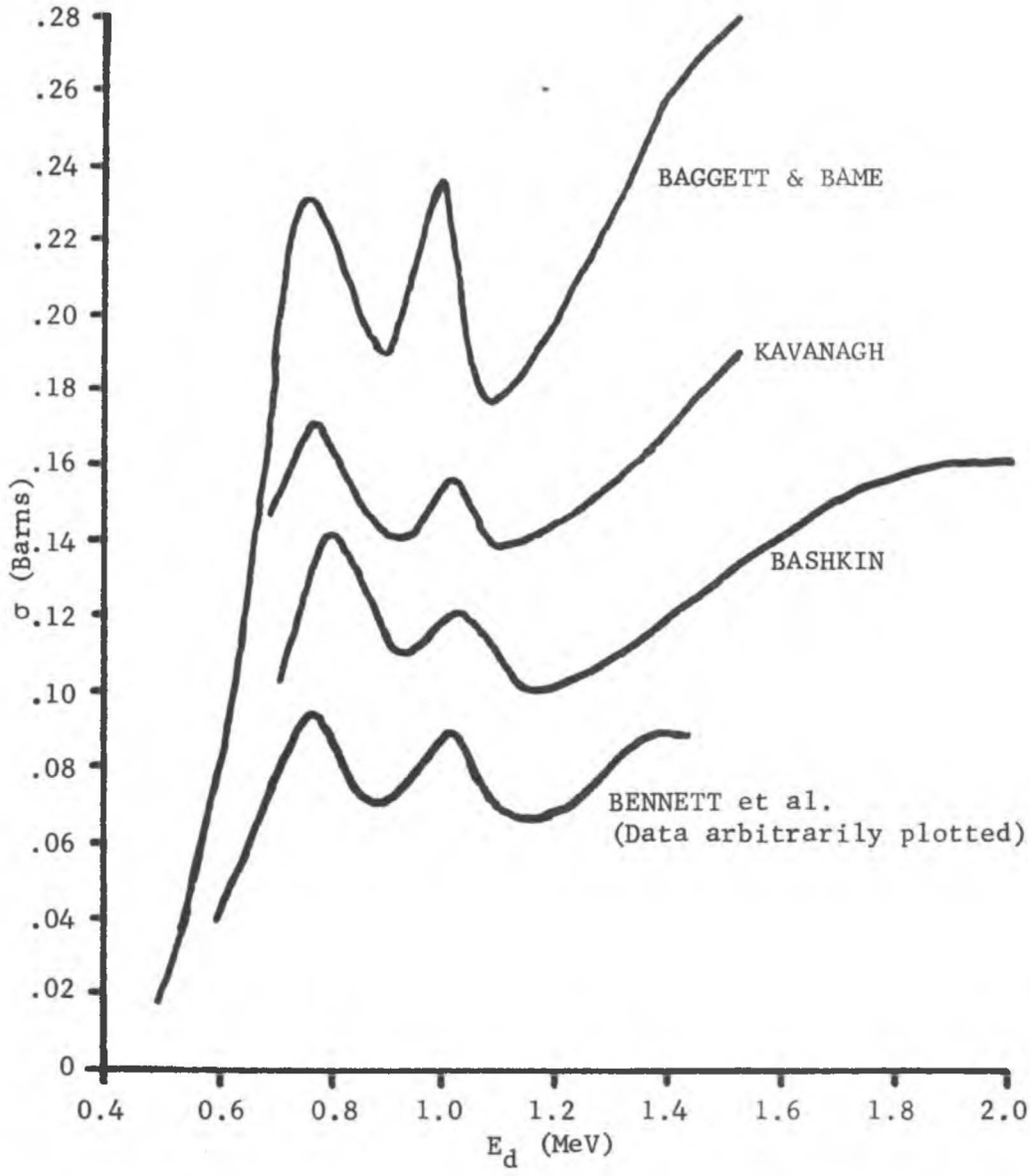

Fig. 3. $^{7}Li(d,p)^{8}Li$ excitation functions by Baggett and Bame[5], Kavanagh[9], Bashkin[6], and Bennett[4] et al.

$^{7}Be(p,\gamma)^{8}B$ reaction, R. W. Kavanagh[9] and P. D. Parker[10] used the $^{7}Li(d,p)^{8}Li$ reaction to determine the amount of radioactive ^{7}Be present in their targets. By counting the beta-particles from the decay of ^{8}Li Kavanagh determined the excitation function for the $^{7}Li(d,p)^{8}Li$ reaction at deuteron energies up to 1.50MeV and reports an absolute cross section of 176 $\pm$ 15mb for the 770KeV resonance. Kavanagh's excitation function is also shown in Figure 3 and does not reveal a resonance at 1.35MeV. Parker, on the other hand, obtained his data by counting the delayed alpha-particles from the break-up of ^{8}Be and reports an absolute cross section of 211 $\pm$ 15mb for this same resonance.

While studying low-Q stripping reactions Woods and Wilkinson[11] were first to observe a resonance at 360KeV in the $^{7}Li(d,p)^{8}Li$ reaction. This observation was later confirmed by Imhof[12] et al. More recently Woods and Wilkinson[13] and Imhof[14] et al. determined the excitation function for the $^{7}Li(d,p)^{8}Li$ reaction at deuteron energies ranging from 0.29MeV to 0.50MeV and 0.20MeV to 0.85MeV respectively. Woods and Wilkinson again observed a resonance at 361KeV and Imhof[14] et al. agree. In both cases measurements were obtained by counting the beta-particles from the decay of ^{8}Li. Their excitation functions are shown together in Figure 4.

Lauritsen and Ajzenberg-Selove[15] have provided a review of the half-life values for the ^{8}Li beta decay through 1965. More recent measurements of the ^{8}Li half-life are reported by Wilkinson[16] et al., Daniel[17] et al. and Claassen[18] et al. Their ^{8}Li half-life values, along with those values from the review by Lauritsen and Ajzenberg-Selove, are listed in Table 2.

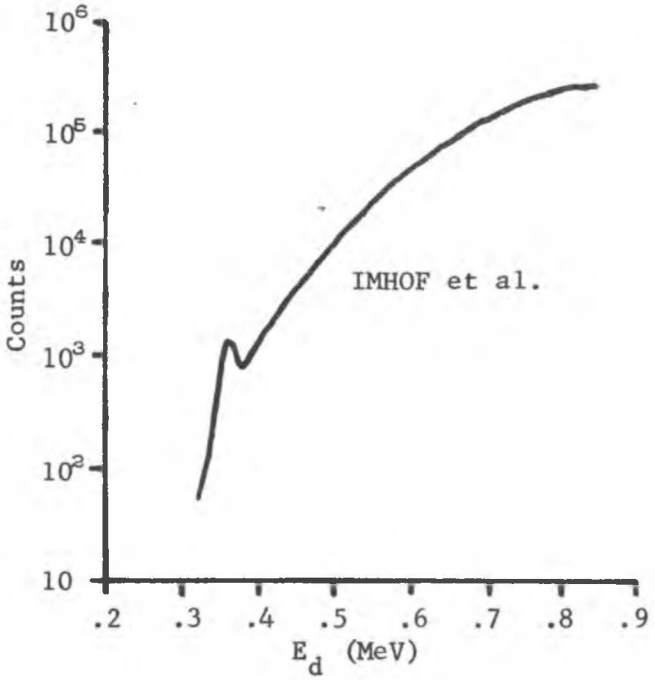

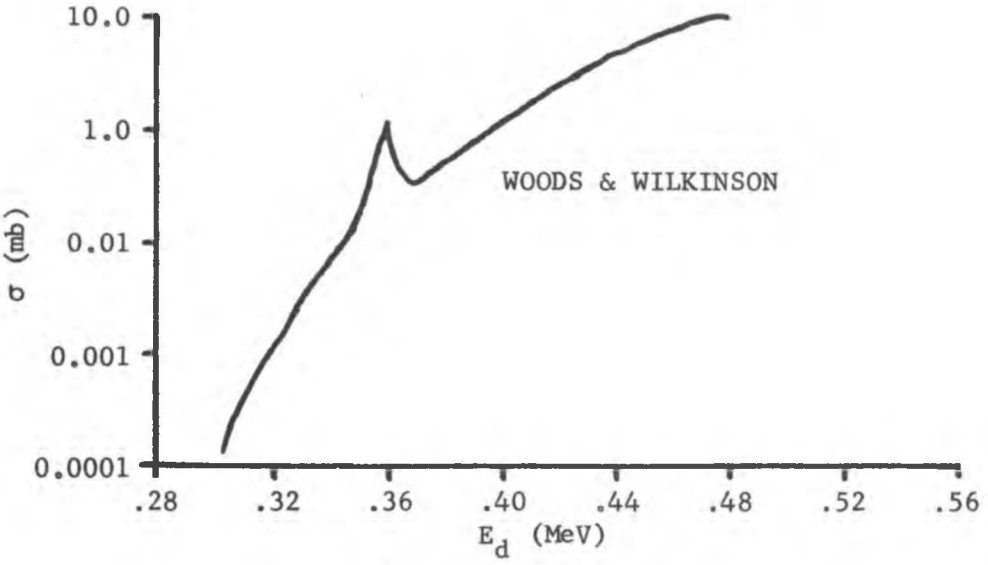

Fig. 4. $^{7}Li(d,p)^{8}Li$ excitation functions by Imhof[14] et al., and Woods and Wilkinson[13].

TABLE 2

HALF-LIFE VALUES FOR THE ^{8}Li BETA DECAY

half-life (secs.)	
0.89 ±0.02	(a)
0.825 ±0.02	(a)
0.89 ±0.01	(a)
0.875 ±0.02	(a)
0.85 ±0.016	(a)
0.84 ±0.04	(a)
0.841 ±0.004	(a)
0.84 ±0.02	(a)
0.88 ±0.03	(a)
0.82 ±0.02	(a)
0.87 ±0.02	(a)
0.849 ±0.004	(b)
0.838 ±0.006	(c)
0.854 ±0.008	(d)
0.8440±0.0007	(e)

a. Values from review by Lauritsen and Selove[15]

b. Weighted mean value by Lauritsen and Selove[15]

c. Wilkinson[16] et al.

d. Daniel[17] et al.

e. Claassen[18] et al.

Summary of Literature Review

The preceeding literature review reveals three resonances for the ^{7}Li(d,p)^{8}Li reaction between deuteron energies of 0.25MeV and 1.10MeV. These three resonances, along with their cross sections, widths and corresponding energy levels in the ^{9}Be compound nucleus, are listed in Tables 3 and 4 respectively.

TABLE 3

CROSS SECTION VALUES AT RESONANCES FOR THE $^{7}Li(d,p)^{8}Li$ REACTION AT DEUTERON ENERGIES RANGING FROM 0.25MeV TO 1.10MeV

E_{res} (MeV)	Cross Section (mb)	
0.361	11.0	(a)
0.770	230	(b)
0.770	150	(c)
0.770	176±15mb	(d)
0.770	211±15mb	(e)
1.02	235	(b)
1.02	120	(c)
1.02	159	(d)

a. Woods and Wilkinson[13]

b. Baggett and Bame[5]

c. Bashkin[6]

d. Kavanagh[9]

e. Parker[10]

TABLE 4

EXPERIMENTAL PARAMETERS FOR THE $^{7}Li(d,p)^{8}Li$ REACTION

E_{res} (MeV)	Width (KeV)	^{9}Be (MeV)
0.361	<2	16.973±0.004
0.770	250	17.28
1.02	60	17.48

Values from review by Lauritsen and Selove[15]

III. EXPERIMENTAL CONSIDERATIONS

This section contains a description of the experimental apparatus and procedures used to determine the excitation function and cross section values for the $^{7}Li(d,p)^{8}Li$ reaction at deuteron energies ranging from 0.623MeV to 1.968MeV (see Appendix B for the energy calibration used in the determination of this excitation function and the corresponding cross section values).

General Information

Faraday Cup.--The faraday cup is a cylindrical iron and aluminum container approximately three inches in diameter and seven inches long. This cup is totally insulated from its surroundings and terminates the deuteron beam. The entrance to the faraday cup is shielded by two magnets in such a manner as to permit the deuteron beam to enter the cup while prohibiting secondary electrons from leaving the cup. The faraday cup enables an absolute integration of the beam to within 0.01%. (See Figure 5.)

Target-Detector Assembly.--The target-detector assembly consists of an aluminum target armature approximately five inches long attached to a mechanical solonoid which enables the target to move vertically in or out of the beam; the target armature and solonoid are mounted to the detector assembly so that the target, when not activated, is exactly 0.919 ± 0.005 inches from the detector. (See Figure 5.)

Silicon Surface Barrier Detector.--The detector used in this study is a silicon surface barrier detector with an active surface area of 300mm^2. The detector operates with a positive 50V bias which results in a depletion depth given by the following expression[19]:

$$\text{depletion depth } (w) = 5.3\text{x}10^{-5}(pV)^{\frac{1}{2}} \qquad (5)$$

where p is in ohm-cm and V is in volts.

Scatter Chamber.--The scatter chamber is a circular aluminum chamber approximately eighteen inches in diameter and eight inches high. This chamber houses the faraday cup and target-detector assembly. (See Figures 5 and 6.)

Beam Stop.--The beam stop is a mechanical instrument located within the beam line which enables the beam to be stopped at specific time intervals. (See Figure 6.)

Cold Trap.--The cold trap is a cylindrical aluminum container attached to a cylindrical copper tube within the beam line. The cold trap is cooled with liquid nitrogen and condenses out oil vapors and other impurities from within the vacuum system. The cold trap also aids in preventing carbon build-up on the target surface. (See Figure 6.)

Heath Logic Pulse System.--The Heath logic pulse system is an electronic device which provides a positive 5V logic pulse that interfaces the repeat cycle timer to the linear gate used to gate the detection system and the Geoscience Analog to Digital Converter (ADC) and Multichannel Analyzer (MCA). (See Figure 7.)

Repeat Cycle Timer.--The repeat cycle timer is a mechanical switching mechanism consisting of four single pole double throw switches operated by a synchronized motor. This cycle timer controls

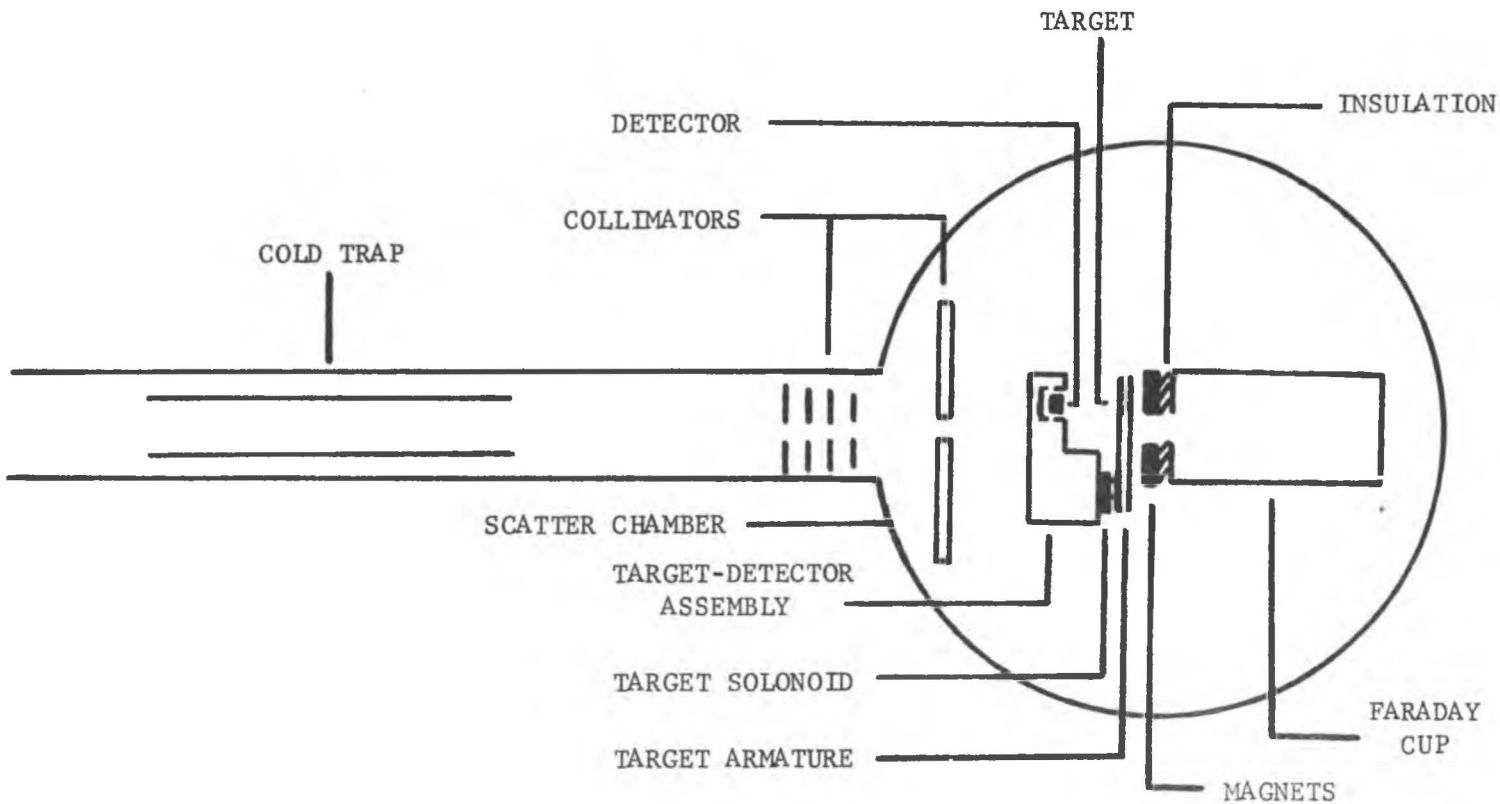

Fig. 5. Physical arrangement of cold trap, collimators, faraday cup, and target-detector assembly.

the beam stop, target solonoid, Heath logic pulse system and detector. (See Figure 7.)

Apparatus and Experimental Arrangement

The 2MeV Van De Graaff Accelerator at Brigham Young University was used to produce a monoatomic deuteron beam with an incident energy ranging from 0.623MeV to 1.968MeV. The beam was energy analyzed using a bending magnet; energy slits along the beam line, coupled to an internal stablizing unit, enabled control over the energy of the beam to within $\pm$5KeV of the desired energy. The physical arrangement of the accelerator, bending magnet, energy slits, beam stop and scatter chamber is shown in Figure 6.

The primary target used in this study was purchased from MicroMatter Co. in Seattle, Washington. This target consists of $104 \pm 2.5 ug/cm^2$ of LiF evaporated on an aluminum backing approximately $700 ug/cm^2$ thick. This target arrangement was thin enough to allow the beam to penetrate the target, but too thick to permit an absolute integration of the beam at the time of irradiation. The $700 ug/cm^2$ aluminum backing was chosen in order to prevent the ^8Li recoils from leaving the target, since range-energy studies[20] and kinematic calculations indicate that at bombarding energies greater than 770KeV ^8Li recoils can penetrate $390 \pm ug/cm^2$ of aluminum backing.

In order to avoid the complications of an in-beam experiment, a cyclic system was devised to count the delayed alpha-particles as a result of the ^8Li beta decay. The electronics for this system, diagrammed in block form, are shown in Figure 7 along with the detection and counting electronics for the overall system. As Figure 7 indicates

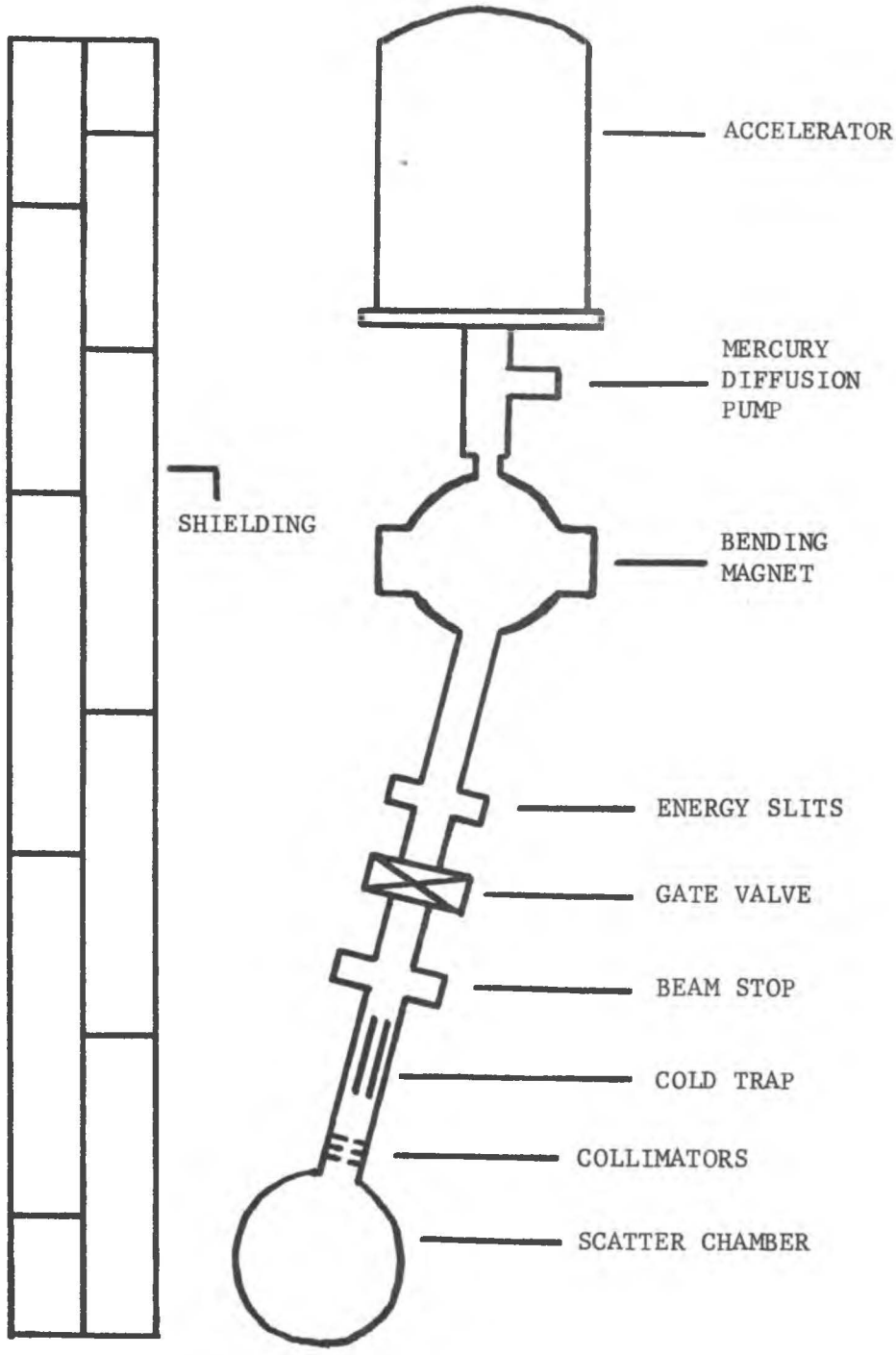

Fig. 6. Physical arrangement of accelerator and related equipment.

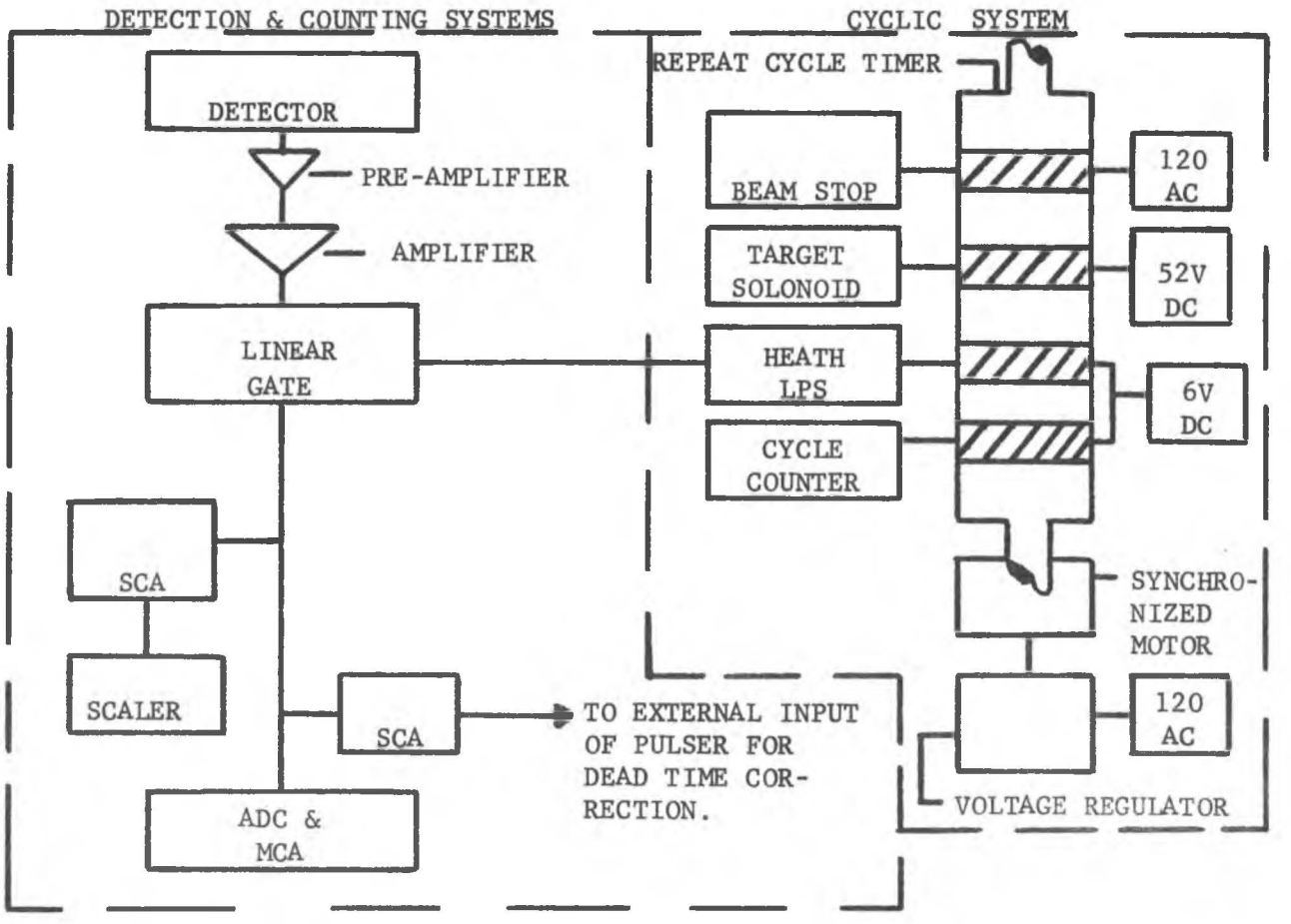

Fig. 7. Block diagram of the electronics for this study illustrating both the cyclic system and detection and counting systems.

the cyclic system consists of a repeat cycle timer, beam stop, target armature solonoid and Heath logic pulse system. This system operates in a cyclic fashion such that irradiation of the target, counting of the target and beam integration occur once every cycle at specific time intervals. The time intervals, measured on a Tektronic Type 454 oscilloscope using the delay multiplier and position of B-time mode, and the cyclic procedure followed in this system are shown in Figure 8. This system then ensures that the target is neither counted nor irradiated while in motion and eliminates all other sources of radiation except the delayed alpha-particles of interest and the beta-particles from the ^{8}Li decay. Since the depletion depth of the detector is so small, the beta-particles do not drop sufficient energy to interfere with the counting of the delayed alpha-particles.

The detection system, shown in Figure 7, was calibrated using alpha-particles from an ^{227}Ac source. The Ortec 431 precision pulser was then normalized to the ^{227}Ac source on the Geoscience ADC and MCA. It was then possible, using the precision pulser, to determine the energy of any channel and the Full Width at Half Maximum (FWHM) for the alpha spectra.

Procedures used in Obtaining Data

The excitation function for the $^{7}Li(d,p)^{8}Li$ reaction was obtained using the $104 \pm 2.5 ug/cm^2$ LiF target previously described. A deuteron beam current of 0.35ua was used. The energy of the beam was increased slowly in 100-200KeV steps using the coarse and fine current control of the magnet power supply until the resonances of interest were approached. Increments of 50-100KeV steps were used over the resonances.

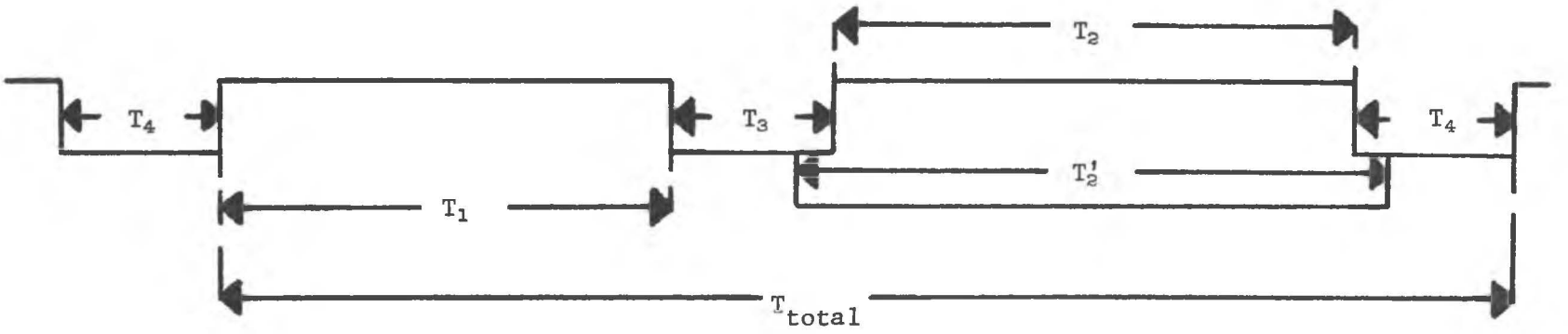

T_1 = Time provided for irradiation of target.

T_2 = Time provided for counting of target.

T_2' = Time provided for beam integration.

T_3 = Time between irradiation and counting of target; target is in motion for first half of T_3.

T_4 = Time between counting and irradiation of target; target is in motion for middle third of T_4.

T_{total} = Total time provided for one cycle.

TIMES	SECONDS
T_{total}	3.934±0.003
T_1	1.643±0.003
T_2	1.634±0.002
T_2'	1.892±0.004
T_3	0.326±0.003
T_4	0.331±0.003

Fig. 8. Schematic illustration of the timing sequence for the cyclic system.

At each magnet setting the cyclic system described in the preceeding section was implimented. During each cycle pulses from the silicon surface barrier detector were simultaneously scaled and energy analyzed in in the Geoscience ADC and MCA (the 1024 channel conversion gain in the ADC being used). Beam integration occurred each cycle using the Ortec 410 current digitizer; the pulses from the digitizer also being scaled each cycle. The length of time spent at each magnet setting varied, depending on the location of that point on the excitation function. Over the resonances of interest, the 770KeV and 1.02MeV resonances, irradiation at each magnet setting continued until 10,000 counts were registered in the peak channel. At the end of each run a readout from the MCA was obtained.

Since the radiation from the LiF target is exponential with respect to time and random with respect to the electronics of the system, standard dead time corrections for the Pulse Height Analyzer (PHA) and remaining electronic systems were not applicable. To correct for the dead time of the entire system a set fraction of the pulses from the detector were delayed and used to externally drive an Ortec 431 presicion pulser. The pulses from this precision pulser were then simultaneously scaled and introduced through the entire system being energy analyzed in the PHA. The 431 precision pulser was then adjusted to fall several hundred channels above the tail of the alpha spectrum. A ratio of the number of pulses energy analyzed to the number of pulses initially scaled provided an accurate dead time correction for the entire system.

IV. DATA ANALYSIS AND EXCITATION FUNCTION

In this section the procedures used to analyze the data and determine the excitation function for the $^{7}Li(d,p)^{8}Li$ reaction are presented. Following the presentation of the data analysis and excitation function a short summary of observed nuclear parameters measured in this study is given.

Data Analysis

Figure 9 through 13, displaying data at deuteron energies of 0.689MeV, 0.762MeV, 0.932MeV, 1.274MeV and 1.728MeV respectively, are representative of the 89 individual delayed alpha-particle spectra, containing no less than 250,000 counts each, used to determine the $^{7}Li(d,p)^{8}Li$ excitation function. These alpha spectra indicate the presence of another delayed emitter within the target material which appears at a maximum in channel 30 and corresponds to particles with an average energy of 0.449MeV. Numerous spectra of this delayed emitter, obtained by energy analyzing this impurity in the Geoscience ADC and MCA, were plotted on the A1029 Hewlett Packard Calculator and Plotter. Analysis of these plots revealed that these impurity spectra fit a gaussian distribution to within 5%. Therefore, since the area under a gaussian distribution is defined as:

$$A = h\int_{-\infty}^{\infty} e^{-kx^2} dx = h(\pi/k)^{\frac{1}{2}} \qquad (6)$$

where h is the height of the gaussian curve and k is a constant depend-

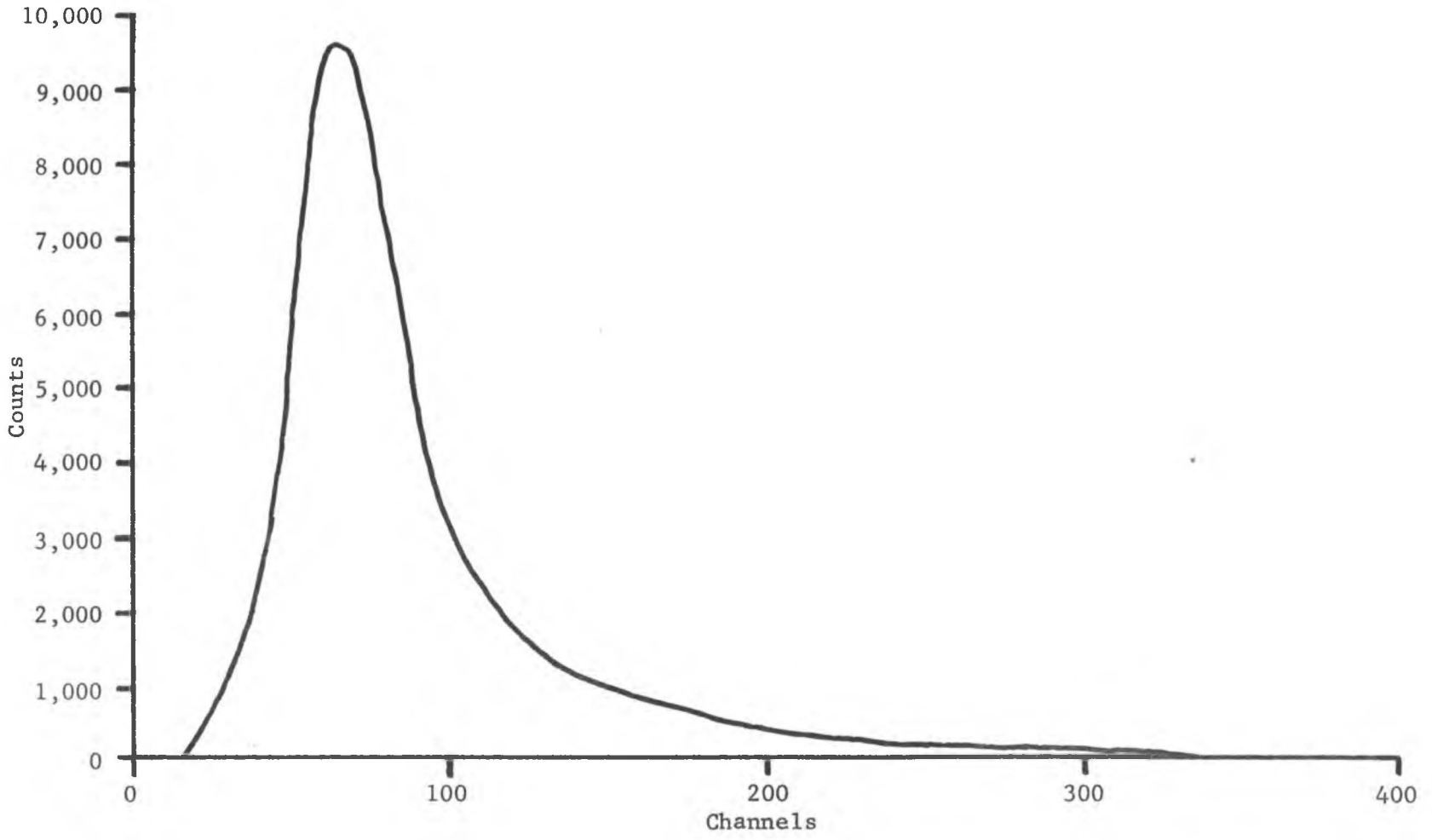

Fig. 9. Delayed alpha spectrum from the decay of the 2.90MeV level of ^{8}Be. This alpha spectrum contains 532,580 total alpha counts. E_d = 0.689MeV.

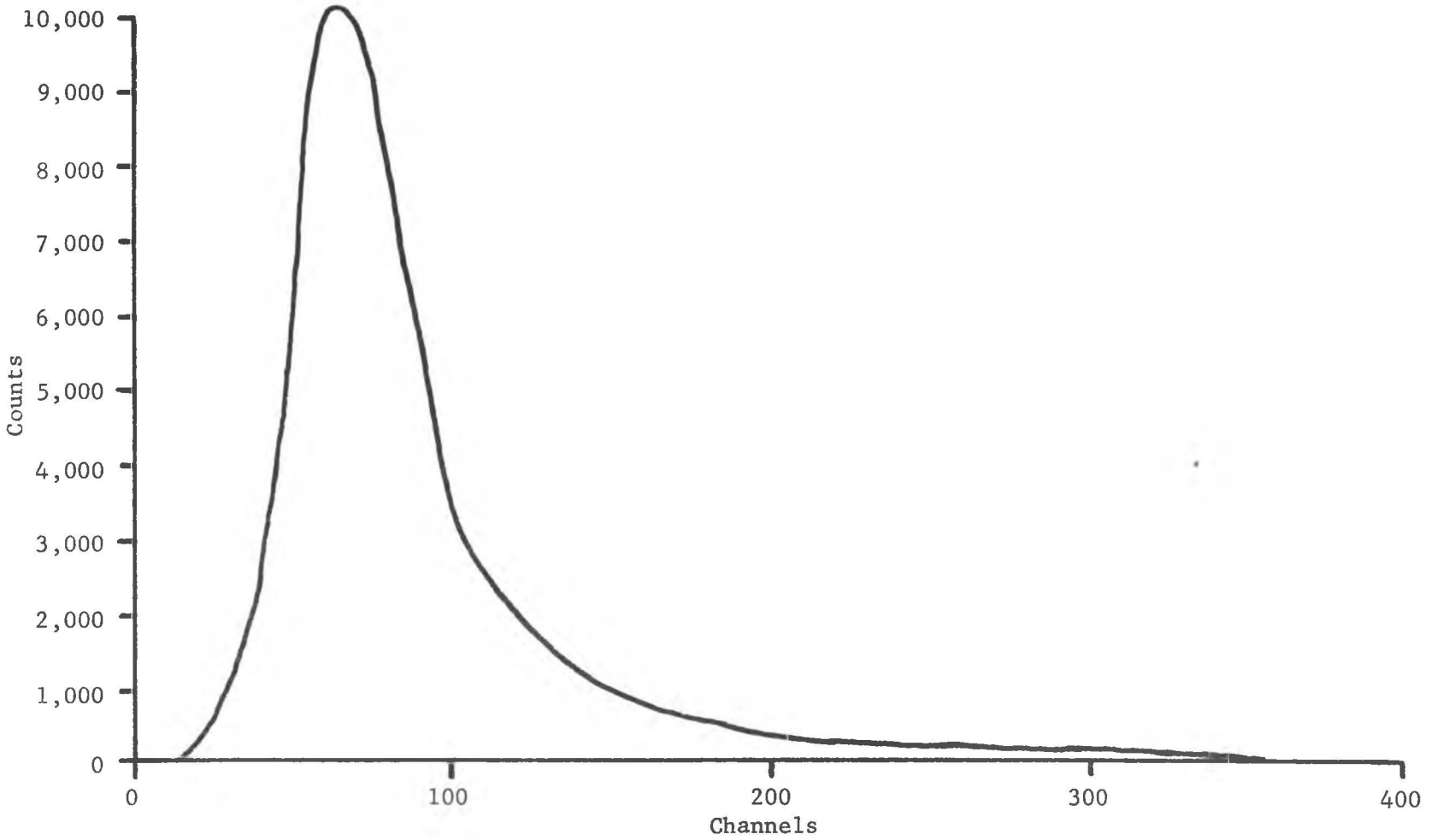

Fig. 10. Delayed alpha spectrum from the decay of the 2.90MeV level of ^{8}Be. This alpha spectrum contains 602,407 total alpha counts. E_d = 0.762MeV.

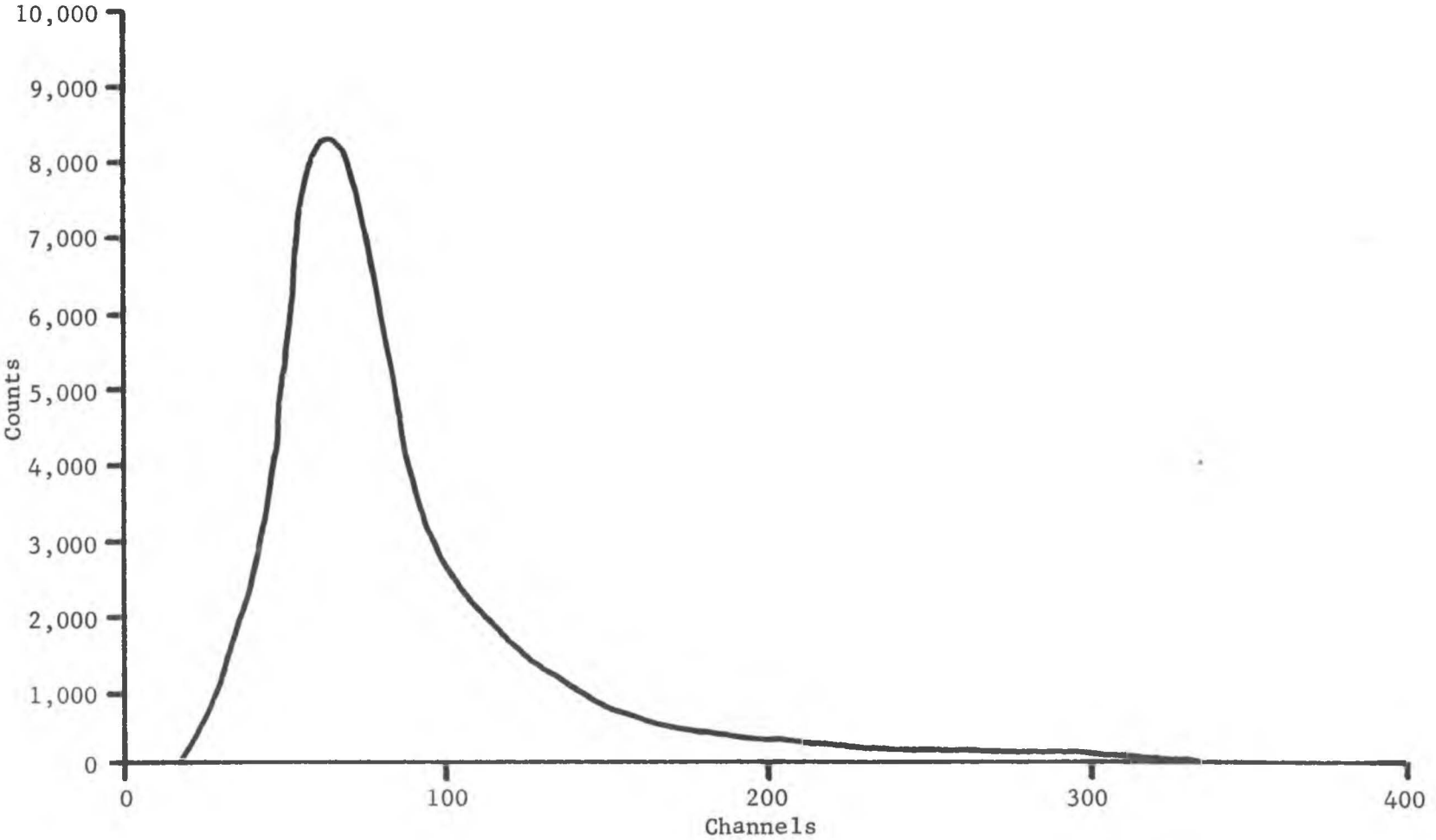

Fig. 11. Delayed alpha spectrum from the decay of the 2.90MeV level of ^{8}Be. This alpha spectrum contains 473,398 total alpha counts. E_d = 0.932MeV.

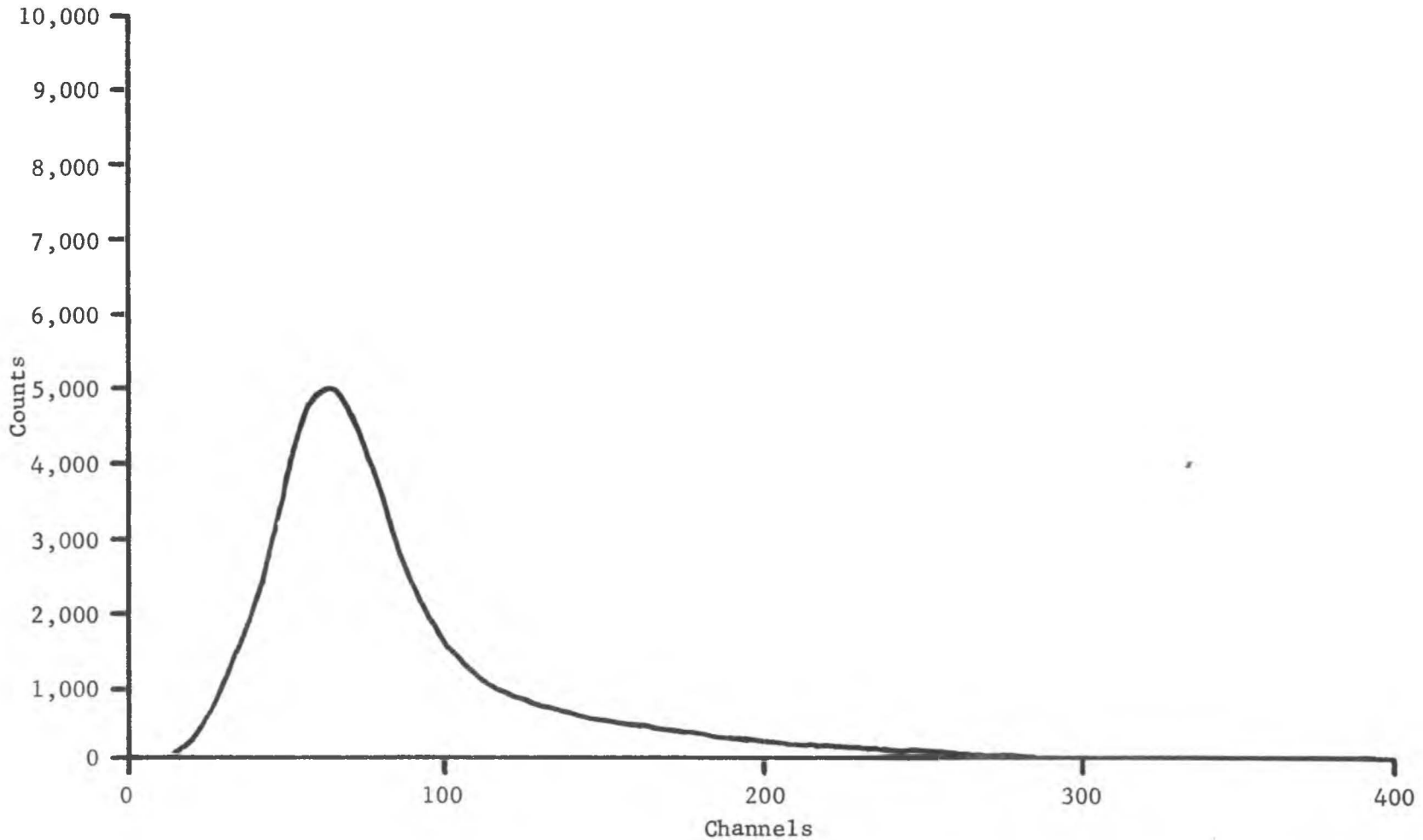

Fig. 12. Delayed alpha spectrum from the decay of the 2.90MeV level of ^{8}Be. This alpha spectrum contains 296,909 total alpha counts. E_d = 1.728MeV.

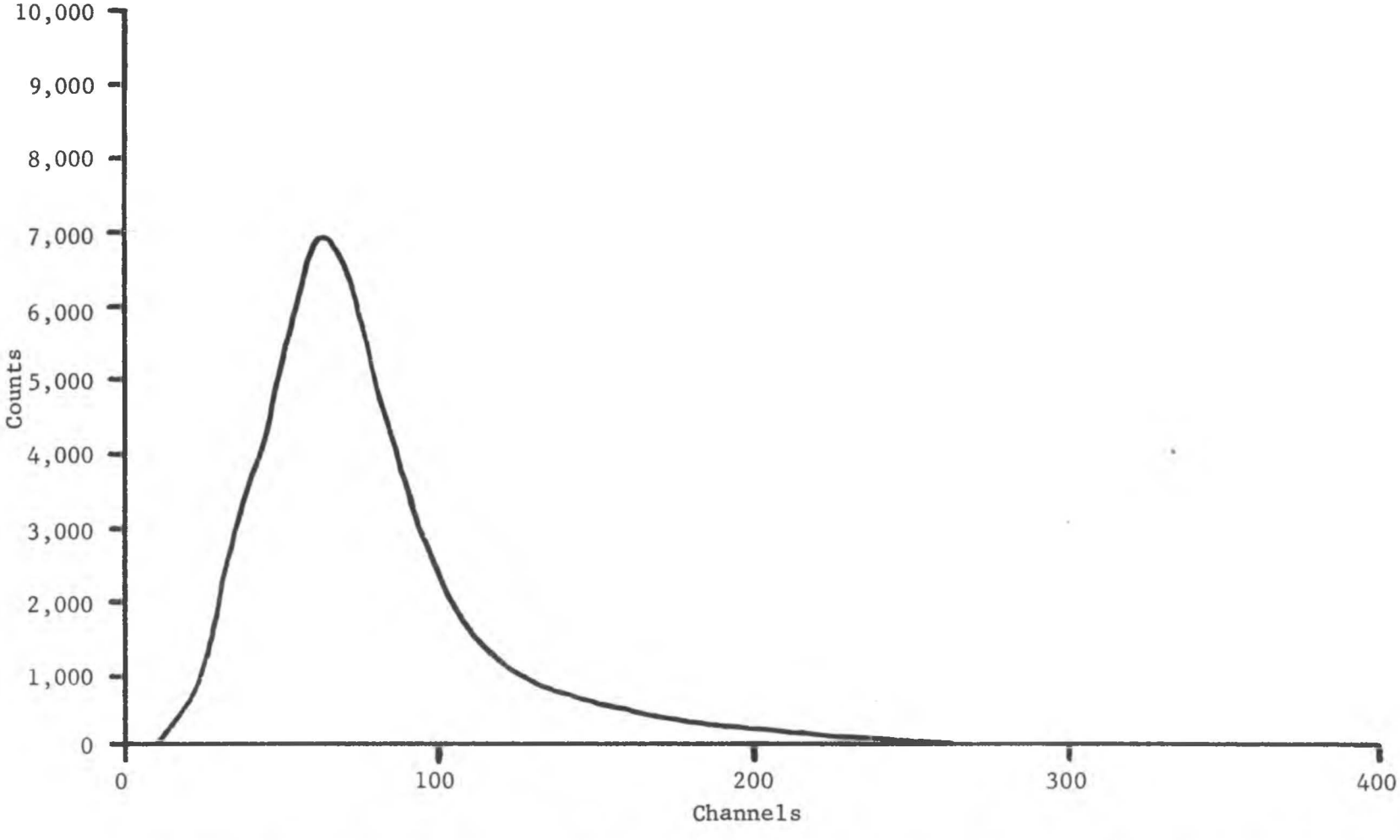

Fig. 13. Delayed alpha spectrum from the decay of the 2.90MeV level of ^{8}Be. This alpha spectrum contains 437,356 total alpha counts. E_d = 1.728MeV.

ing on the height and width of the gaussian curve, each of the 89 individual alpha spectra must be corrected for this impurity using equation 6; hence, the height and k value for the impurity within each alpha spectrum must be determined.

Following this procedure the height of the impurity within sixteen alpha spectra was empirically determined by subtracting an estimated height until the proper alpha peak shape was obtained. Figures 14 through 17 are representative of this procedure and clearly show the height of the impurity and the resultant shape of the alpha spectra after subtraction of the impurity. Using these sixteen plotted spectra and the corresponding heights of the impurity within these spectra a plot of the ratio (K) of the number of counts in channel 30 to the average number of counts in the peak channel versus magnet current was made. This plot is shown in Figure 18 and indicates that the height of the impurity can be determined within 1%.

In order to determine the k value (eq. 6) for the impurity within each alpha spectrum, a plot of the height of the impurity versus the k value for four impurity spectra was made. This plot is shown in Figure 19 and indicates that the k value can be determined from this plot within 0.5%; thereby showing that the area under a gaussian distribution of a particular height can be determined to well within 2%.

Using Figures 18 and 19 the area due to the impurity within each alpha spectrum was obtained and subsequently subtracted. From these corrected alpha spectra the total cross section corresponding to each spectrum was calculated using the cross section equation given in Appendix A and the ^{8}Li half-life value reported by Woods and Wilkinson[13].

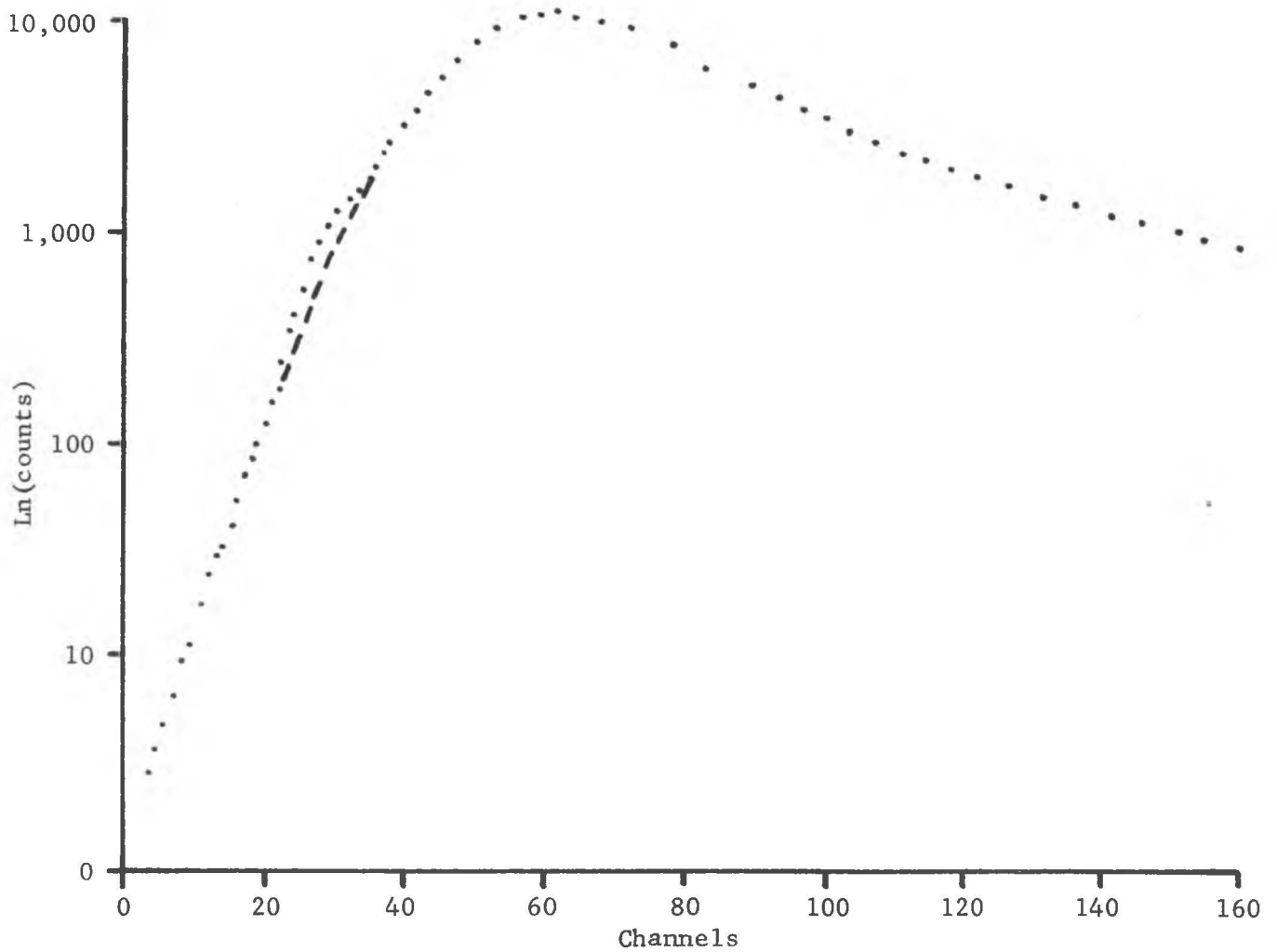

Fig. 14. Logarithmic plot of delayed alpha spectrum showing the presence of another delayed emitter. Black dashed line indicates the subtraction of the impurity corresponding to a height of 207 counts. E_d = 0.689 MeV.

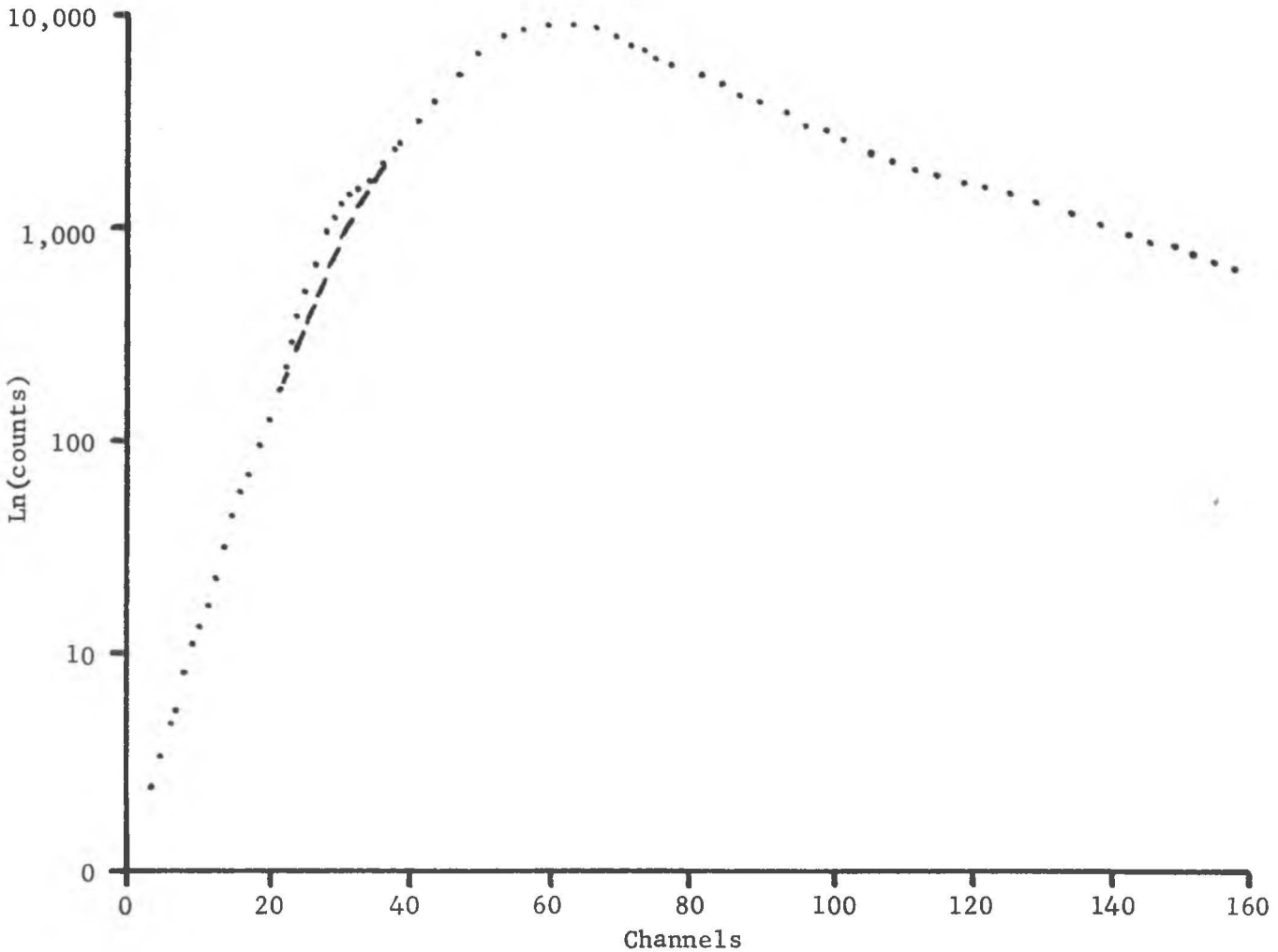

Fig. 15. Logarithmic plot of delayed alpha spectrum showing the presence of another delayed emitter. Black dashed line indicates the subtraction of the impurity corresponding to a height of 207 counts. E_d = 0.762MeV.

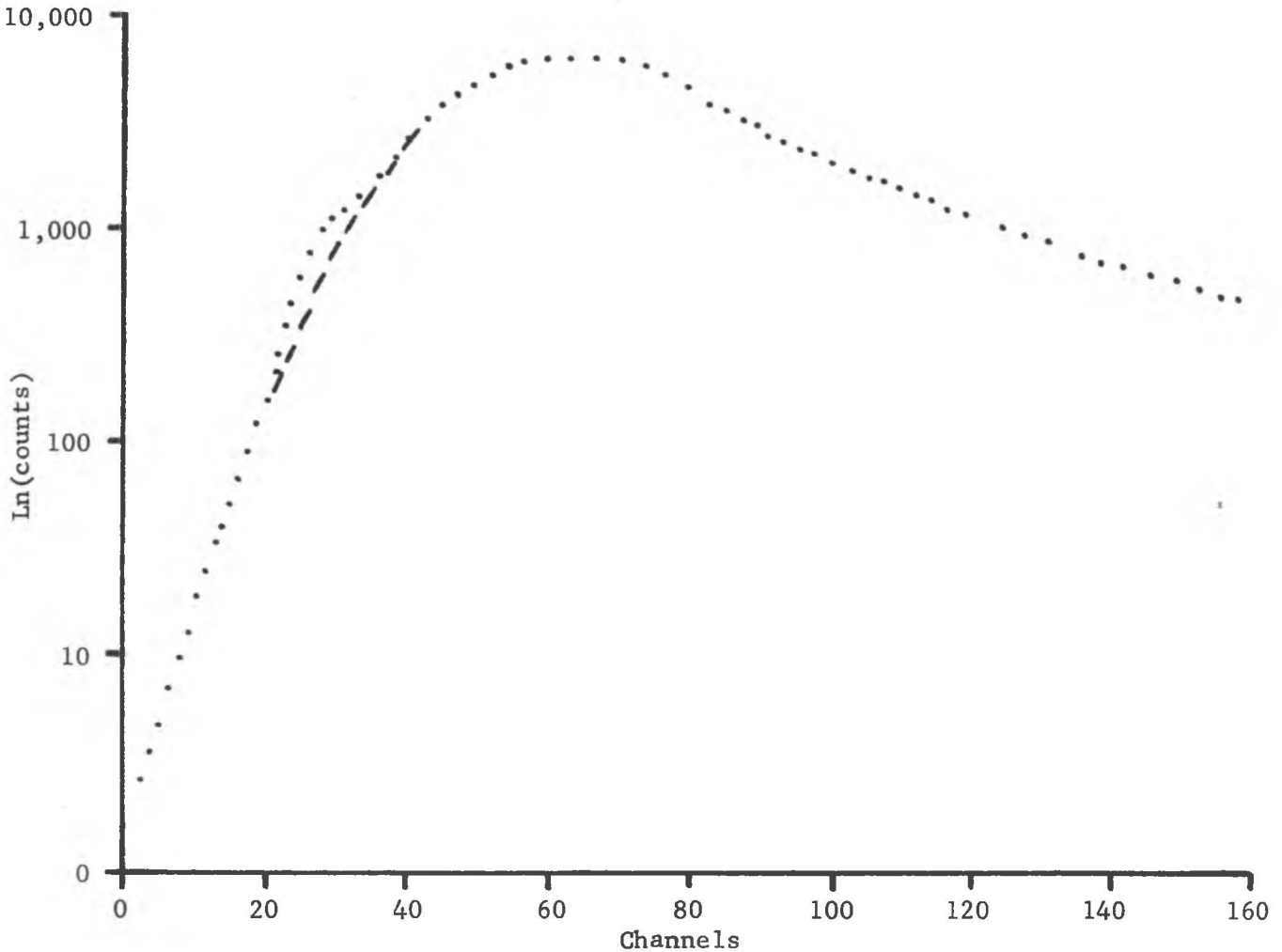

Fig. 16. Logarithmic plot of delayed alpha spectrum showing the presence of another delayed emitter. Black dashed line indicates the subtraction of the impurity corresponding to a height of 275 counts. E_d = 0.932MeV.

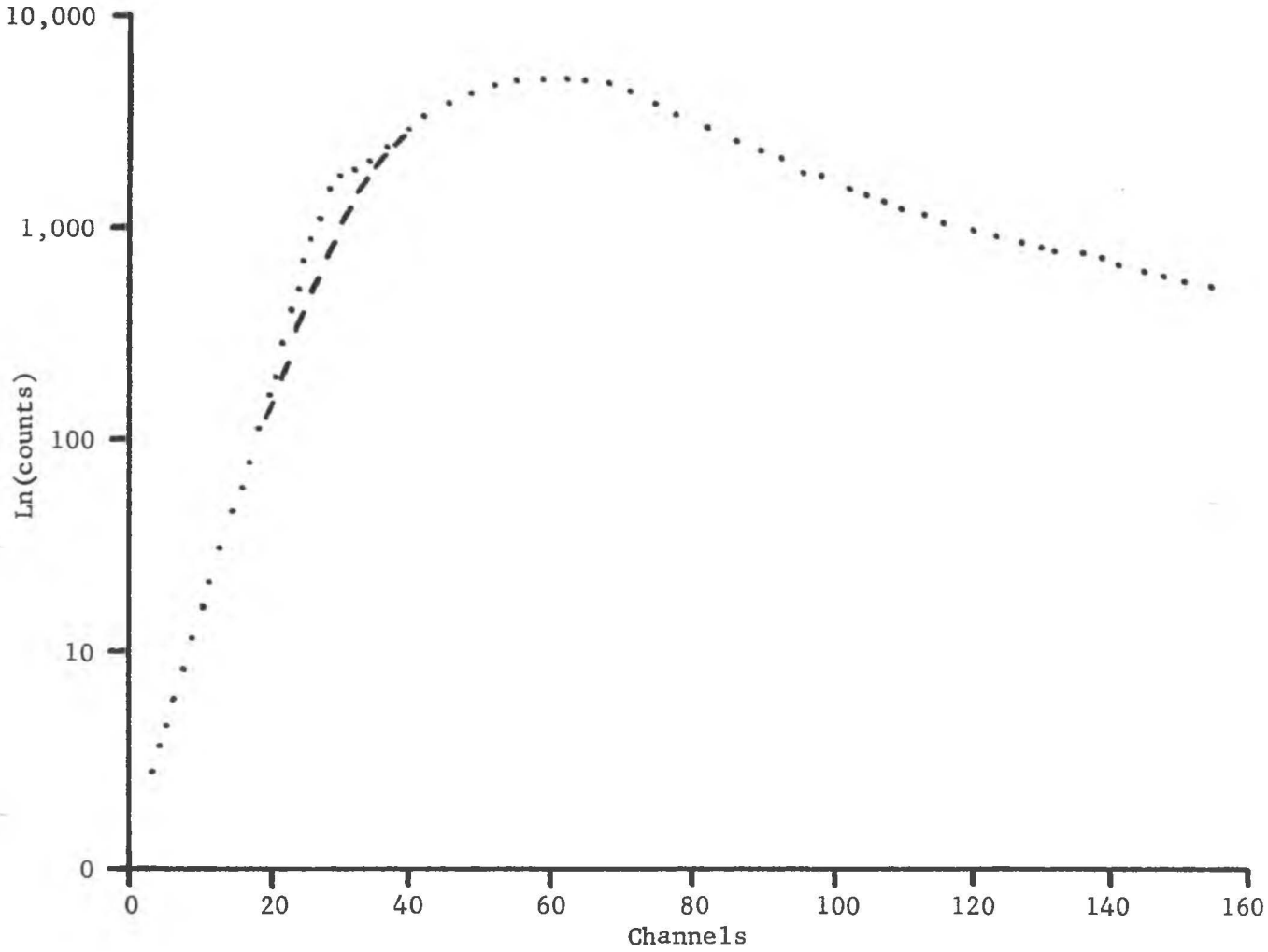

Fig. 17. Logarithmic plot of delayed alpha spectrum showing the presence of another delayed emitter. Black dashed line indicates the subtraction of the impurity corresponding to a height of 431 counts. E_d = 1.728MeV.

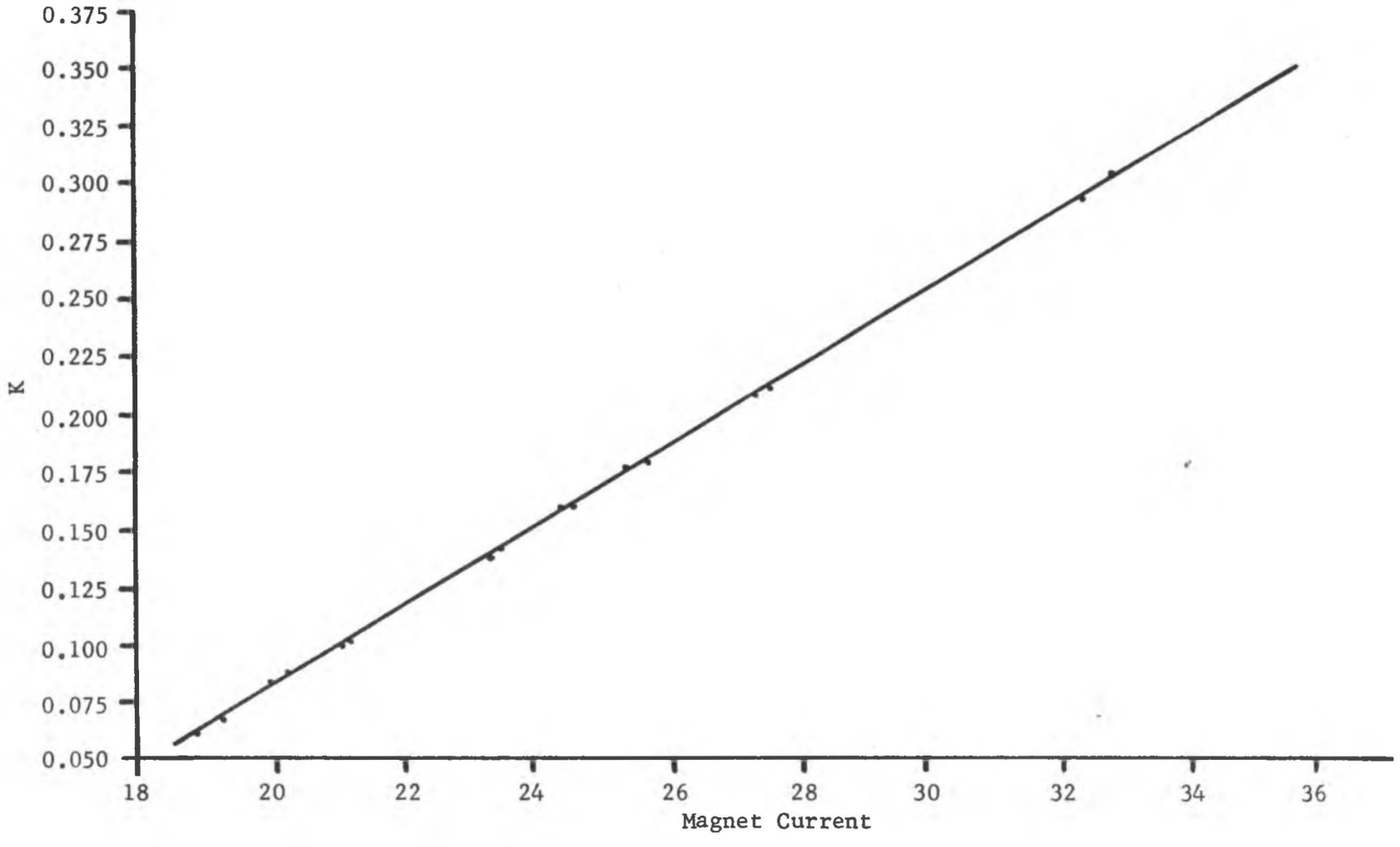

Fig. 18. Plot of the ratio (K) of the number of counts in channel 30 to the average number of counts in the peak channel versus the magnet current for sixteen alpha spectra. This plot indicates that the height of the impurity can be determined within 1%.

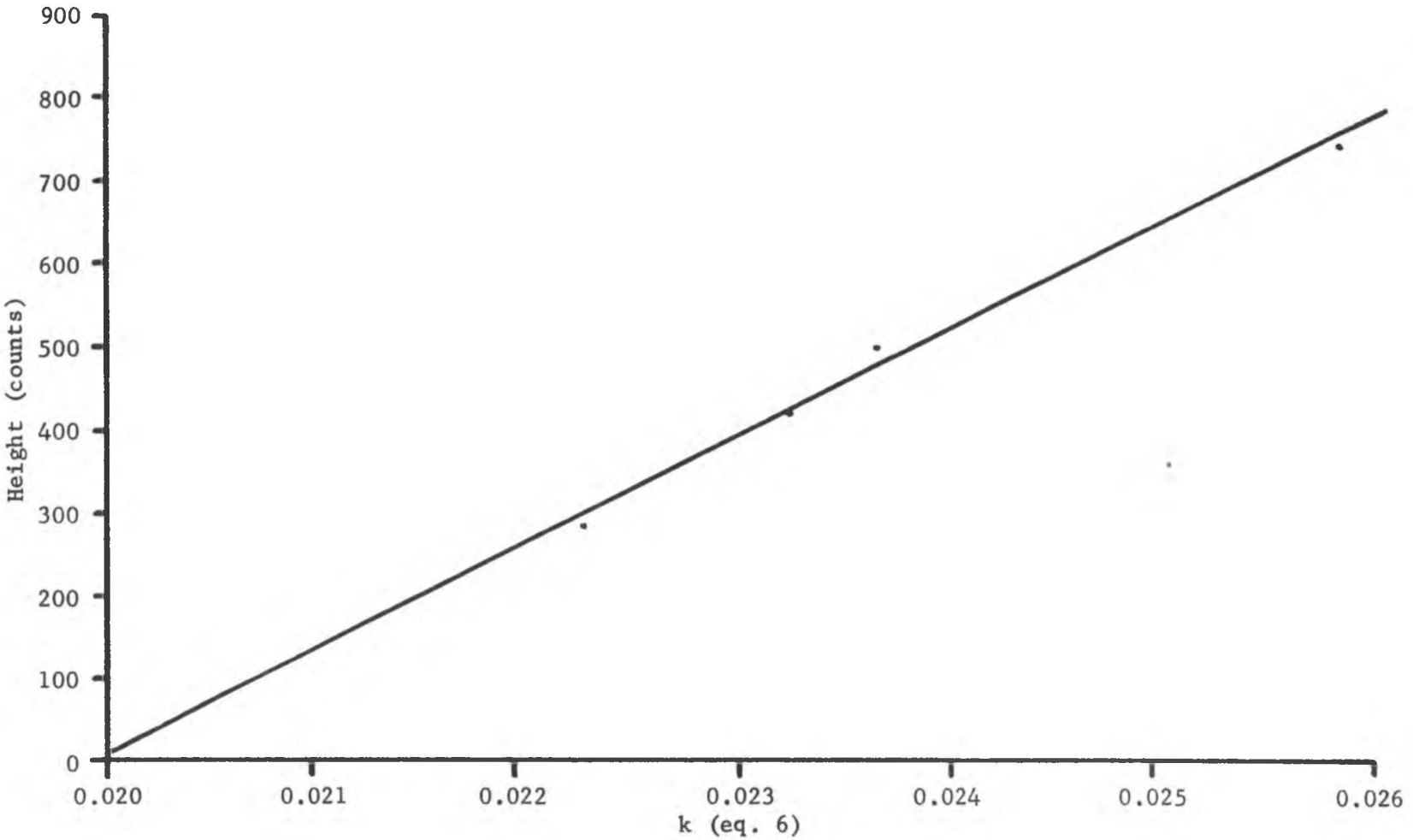

Fig. 19. Plot of the height of the impurity versus the k value (eq. 6) for four impurity spectra. This plot indicates that the k value can be determined within 0.5%.

$^{7}Li(d,p)^{8}Li$ Excitation Function

The excitation function for the $^{7}Li(d,p)^{8}Li$ reaction at deuteron energies ranging from 0.623MeV to 1.968MeV is shown in Figure 20. Points on this excitation function, indicating resonances at 0.777 ± 0.012MeV and 1.031 ± 0.015MeV with cross sections of 202 ± 9mb and 188 ± 8mb respectively, were reproducible to within 0.5% after removal and subsequent replacement of the target and target-detector assembly.

The uncertainty in these cross section values was determined from the three independent sources of error within this experiment, the solid angle, the ^{8}Li half-life, and the target thickness. The uncertainties in the solid angle and target thickness are $\pm 1.1\%$ and $\pm 2.5\%$ respectively. The uncertainty in the ^{8}Li half-life, using the value reported by Woods and Wilkinson[13], is $\pm 0.6\%$. Combining these uncertainties results in an overall uncertainty of $\pm 4.2\%$. No correction to the resonance and non-resonance cross sections due to target thickness effects[21] was made since theoretical calculations indicate that only relative corrections could be made.

The uncertainty in the energy values associated with this excitation function are discussed in Appendix B. All other sources of error, such as dead time in the electronics, mechanical uncertainties, and timing uncertainties were corrected or proven to be negligible.

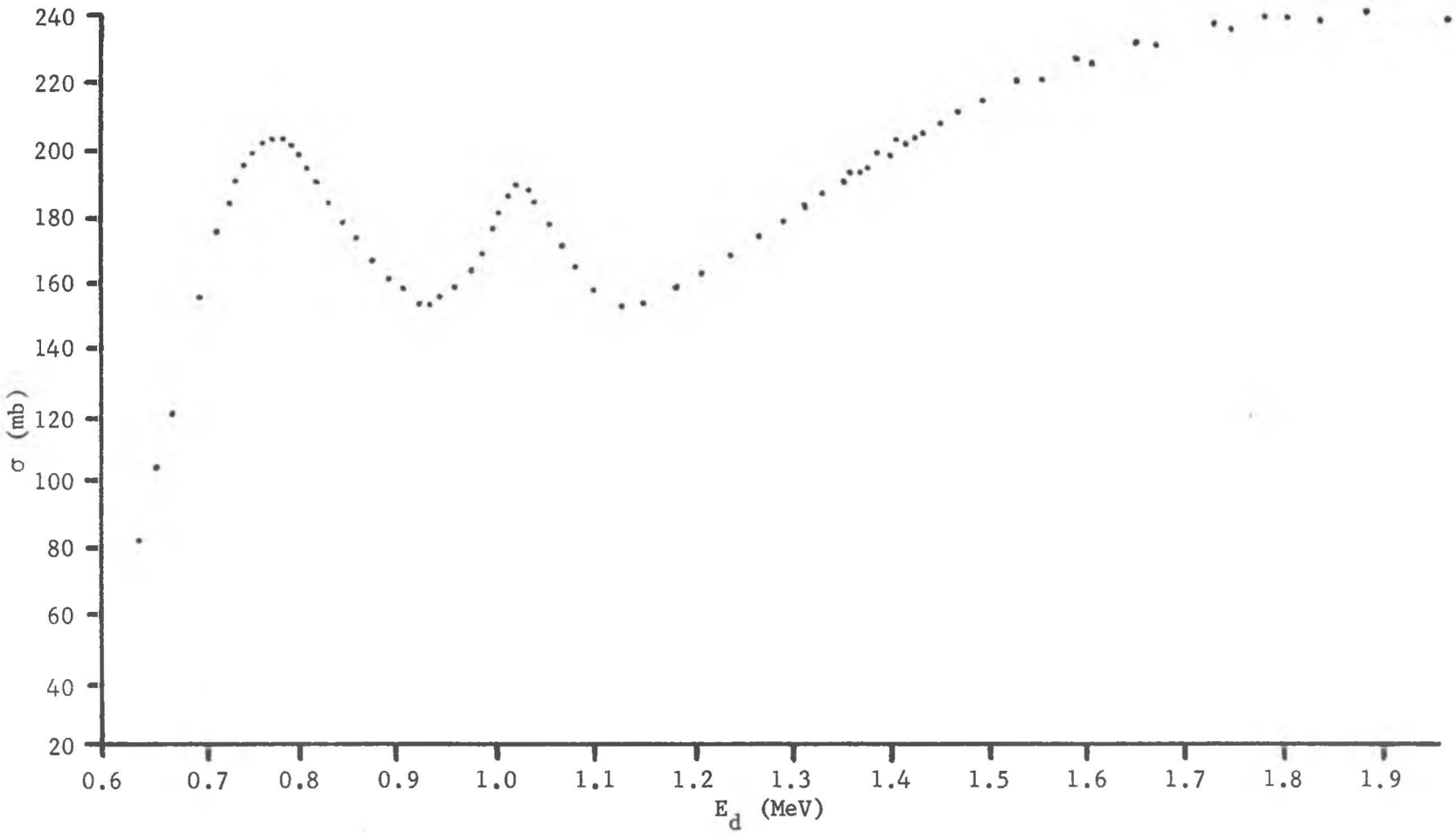

Fig. 20. Excitation function for the $^{7}Li(d,p)^{8}Li$ reaction at deuteron energies ranging from 0.623MeV to 1.968MeV. This excitation function reveals resonances at 0.777 ± 0.012MeV and 1.031 ± 0.015MeV.

Summary of Nuclear Parameters

During the course of this study several nuclear parameters associated with the $^{7}Li(d,p)^{8}Li$ reaction have been measured. These measured nuclear parameters are listed in Tables 5 and 6 along with statements on the validity of these values.

TABLE 5

CROSS SECTION AND WIDTHS OF RESONANCES FOR THE $^{7}Li(d,p)^{8}Li$ REACTION

E_{res} (MeV)	Cross Section (mb)	Width (KeV)
0.777 ± 0.012	202 ± 9	180 (a)
1.031 ± 0.015	188 ± 8	63 (a)

a. In order to obtain these values the non-resonance background was estimated; therefore, these values serve only to verify that the proper resonances have been investigated.

TABLE 6

MEASURED NUCLEAR PARAMETERS OF THE $^{7}Li(d,p)^{8}Li$ REACTION

^{8}Li Half-life (secs.)	Width of 2.90MeV Level of ^{8}Be
0.838 ± 0.018 (a)	1.434MeV (b)

a. This value was not used in the cross section calculation due to the large uncertainty.

b. Averaged FWHM of 89 alpha spectra. This value is uncertain due to target thickness effects and energy loss of alpha-particles emerging from target.

V. DISCUSSION

This section contains a discussion of target thickness effects on the $^{7}Li(d,p)^{8}Li$ excitation function, the width of the 2.90MeV level in ^{8}Be and the widths of the 17.28MeV (0.777MeV resonance) and 17.48MeV (1.031MeV resonance) levels in ^{9}Be.

Target Thickness Effects

To a simple approximation the total cross section for the $^{7}Li(d,p)^{8}Li$ reaction at any point on the excitation function can be considered as being the sum of the resonance cross section plus the non-resonance or direct reaction cross section. In order to determine the total cross section, the resonance cross section (σ_r) and the direct reaction cross section (σ_{dr}) must be separately determined from the total cross section and individually corrected for target thickness effects if applicable.

In the course of this study target thickness effects on both the resonance and non-resonance cross sections were considered. In Figure 21 the excitation function for the $^{7}Li(d,p)^{8}Li$ reaction in terms of total cross section values and the estimated non-resonance background are shown. The difference between these two excitation functions gives the resonance excitation function which is shown in Figure 22. Since the FWHM values for the 0.777MeV and 1.031MeV resonances, shown in Figure 22, agree to within 8% of the values reported from the review by

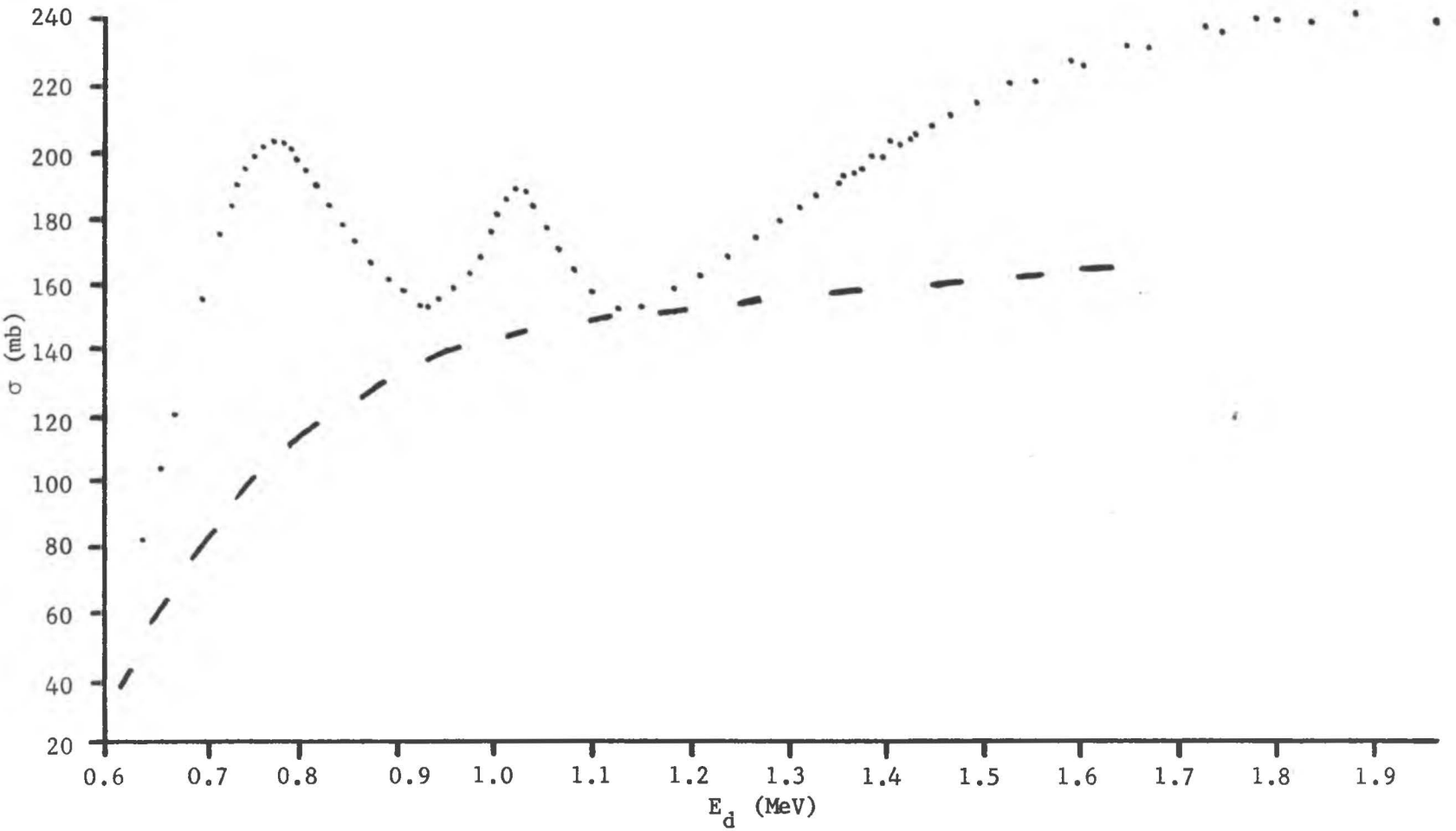

Fig. 21. Excitation function for the $^{7}Li(d,p)^{8}Li$ reaction. Dashed line indicates the estimated non-resonance background for this reaction. Subtraction of these two excitation functions is shown in Figure 22.

Lauritsen and Selove,[15] the non-resonance background, shown in Figure 21, is assumed valid to at least 20%.

Using the resonance cross section values shown in Figure 22 the resonance cross section can be corrected for target thickness effects according to theoretical calculations by Fowler et al.[21] Following their procedure the particle or gamma-ray yield for a nuclear reaction, neglecting wave length and penetration factors, is defined as:

$$Y = \int_{E-\mathcal{E}}^{E} \sigma/\epsilon \, dE \qquad (8)$$

where ϵ is the stopping cross section for the incident particle per disintegrable nucleus in the target material and $\mathcal{E}$ is the energy loss per incident particle in the target material (at incident deuteron energies of 0.777MeV and 1.031MeV $\mathcal{E}$ is 39KeV and 33KeV respectively).[22] Using the Breit-Wigner dispersion equation for the cross section (σ),

$$\sigma = \sigma_r(\Gamma^2/4)/[(E-E_r)^2+(\Gamma^2/4)] \qquad (9)$$

where is the FWHM for the resonance in question, the hield after integration becomes:

$$Y = \frac{\sigma_r \Gamma}{2\epsilon} \left(\tan^{-1}\frac{(E-Er)}{\Gamma/2} - \tan^{-1}\frac{(E-Er-\mathcal{E})}{\Gamma/2}\right) \qquad (10)$$

For any given $\mathcal{E}$, equation 10 has a maximum at $E = E_r + \mathcal{E}/2$ which defines the maximum yield for a resonance reaction as:

$$Y_{max}(\mathcal{E}) = \sigma_{r\Gamma}/(\tan^{-1}\mathcal{E}/\Gamma)\epsilon^{-1} \qquad (11)$$

In the course of this study equation 11 was used to calculate the theoretical yield for the $^{7}Li(d,p)^{8}Li$ reaction at the 0.777MeV and 1.031MeV resonances, but agreement with experimental results was not

obtained. However, agreement to within 33% of the theoretical yield was achieved by taking into account the spins of the interacting particles or the statistical weight factor. The Breit-Wigner dispersion equation (eq. 9), after this modification, then becomes:

$$\sigma = \frac{\sigma_r(2J+1)}{(2I_a+1)(2I+1)} \times (\Gamma^2/4)/[(E-E_r)^2+(\Gamma^2/4)] \quad (12)$$

where J is the total angular momentum of the ^{9}Be compound nucleus, I_a is the spin of the incident particle and I_x is the spin of the target nucleus. A plot of the Breit-Wigner dispersion equation versus energy, shown in Figure 23, illustrates the excellent relative agreement between this dispersion equation and the experimental resonance excitation function; thus confirming the assumption that the Breit-Wigner dispersion equation follows the cross section for a resonance reaction.[21]

Since the theoretical yield cannot be calculated to better than 33% of the experimental yield for both resonances, but good relative agreement was observed, no absolute correction to the resonance cross section was made. Similarly, analysis of the non-resonance excitation function, correlated with energy loss through the target, reveals that at incident deuteron energies above the 1.031MeV resonance no correction is necessary and at deuteron energies less than the 1.031MeV resonance only relative corrections can be made.

Widths in ^{8}Be and ^{9}Be

As previously indicated the ^{7}Li(d,p)^{8}Li excitation function was determined by counting the delayed alpha-particles as a result of the ^{8}Li beta decay. This decay scheme, illustrated in Figure 1, shows the recoil ^{8}Li decaying to the 2.90MeV level of ^{8}Be which subsequently

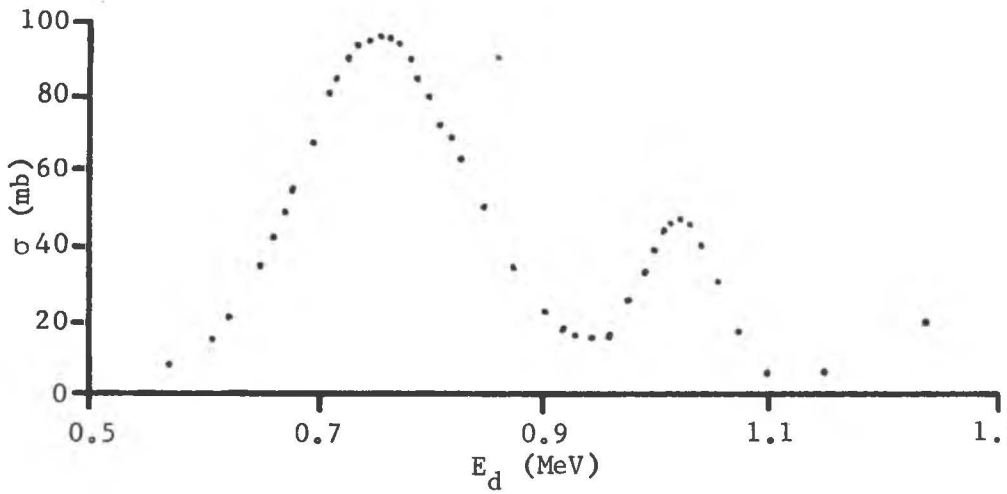

Fig. 22. Plot of the resonance excitation function for the $^{7}Li(d,p)^{8}Li$ reaction.

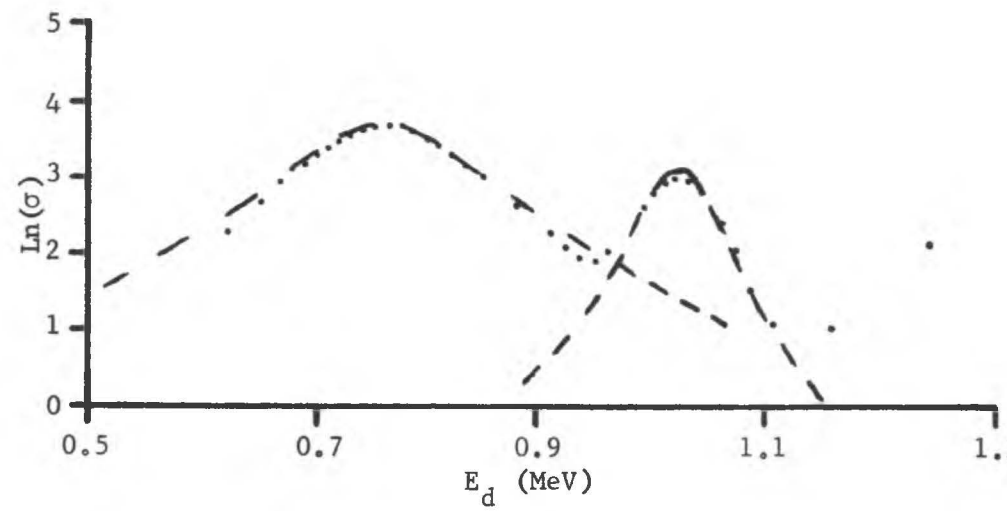

Fig. 23. Logarithmic plot of the Breit-Wigner dispersion equation and the experimental resonance excitation function. Black dashed line indicates the Breit-Wigner dispersion equation; black dotted line indicates the resonance excitation function shown in Figure 22.

breaks apart into two 1.497MeV alpha-particles. Averaging the FWHM values for all 89 alpha spectra used to determine the $^{7}Li(d,p)^{8}Li$ excitation function results in a width of 1.434MeV for the 2.90MeV level in ^{8}Be. However, analysis of these 89 alpha spectra reveals that the peak channel migrates to lower energies as the incident deuteron energy is increased. This migration is not a gain shift, but is due to ^{8}Li recoils penetrating further and further into the target backing which causes the emergent alpha-particles to lose energy. Therefore, while this value is consistent with other reported values,[15] it is an estimated width of the 2.90MeV level and serves only to verify that the proper decay channel was analyzed.

The widths of the 17.28MeV (0.777MeV resonance) and 17.48MeV (1.031MeV resonance) levels within the ^{9}Be compound nucleus were also measured in the course of this study. As indicated in Figure 22 the width of the 0.777MeV resonance, after subtraction of the non-resonance background, is 180KeV and the corresponding width of the 1.031MeV resonance is 63KeV. Because of the estimated non-resonance background, these widths are an estimation and serve only to verify that the proper resonances were analyzed since these widths agree with other reported values.[15]

VI. SUMMARY

In the course of this study the excitation function for the $^{7}Li(d,p)^{8}Li$ reaction was experimentally determined at deuteron energies ranging from 0.623MeV to 1.968MeV by counting the number of delayed alpha-particles as a result of the ^{8}Li beta decay. This excitation function indicates resonances at 0.777 ± 0.012MeV and 1.031 ± 0.015MeV with absolute cross sections of 202 ± 9mb and 188 ± 8mb respectively.

The uncertainty in these cross section values is due to three independent sources of error within this experiment, the solid angle, the ^{8}Li half-life, and the target thickness. Absolute corrections to the resonance and non-resonance cross sections for target thickness effects[21] were considered, but since only relative corrections were possible from the theoretical calculations of Fowler et al.[21], absolute corrections were not made.

The uncertainty in the energy values associated with these cross sections was determined from an energy calibration of the accelerator used in this study. This energy calibration was made using the 1.882MeV resonance from the $^{7}Li(p,n)^{7}Be$ reaction, the 0.770MeV and 1.02MeV resonances from the $^{7}Li(d,p)^{8}Li$ reaction, and the 0.837MeV resonance from the $^{19}F(p,\alpha\gamma)^{16}O$ reaction.

The widths of the 2.90MeV level in ^{8}Be, the 17.28MeV level in ^{9}Be, and the 17.48MeV level in ^{9}Be were measured in this study. Since these values, listed on page 38 of this text, are an estimation, but

agree with previously reported values,[15] they indicate that the proper decay channel and resonances were analyzed.

APPENDIX A

MATHEMATICAL DERIVATION OF CROSS SECTION AND DEFINITION OF SYMBOLS

This appendix contains the mathematical derivation of the cross section used in this study. Following this derivation an explanation of the symbols used in this derivation is presented.

DERIVATION OF CROSS SECTION EQUATION[23]

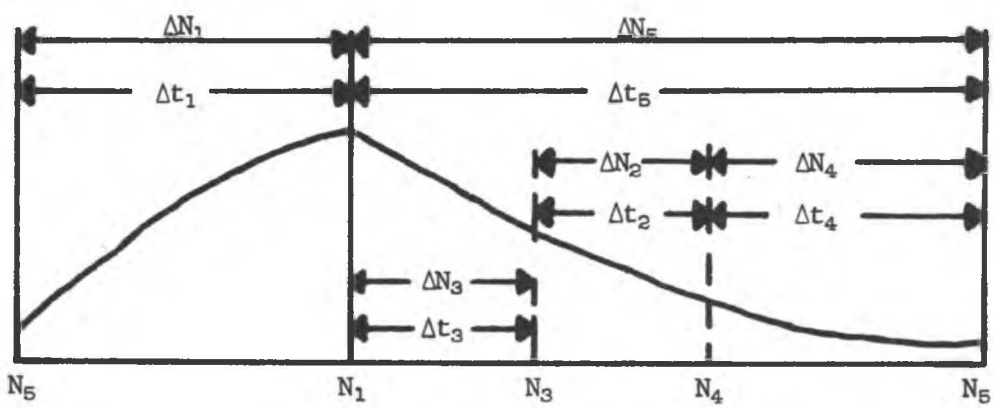

Fig. 24

Figure 24 schematically illustrates the radioactive build-up during irradiation of the target (Δt_1) and its subsequent decay following this irradiation (Δt_5). For this system, shown in figure 24, the following equations result:

$$\Delta N_5 = N_5 - N_1 \qquad (1)$$

$$\Delta N_1 = N_1 - N_5 \qquad (2)$$

$$\Delta N_3 = N_3 - N_1 \qquad (3)$$

$$\Delta N_4 = N_5 - N_4$$

$$\Delta N_2 = N_4 - N_3 \tag{5}$$

$$\Delta N_5 = -\Delta N_1 \tag{6}$$

Using these six equations and the two basic equations for radioactive decay and bombardment, equations[2] 7 and 8 respectively, the derivation of the cross section equation proceeds as follows:

$$N = N_0 e^{-\lambda t} \qquad \text{(for decay)} \tag{7}$$

$$Q - \lambda N = (Q - \lambda N_0)_{t=0} e^{-\lambda t} \qquad \text{(for bombardment)} \tag{8}$$

---

from eq. 7:

$$N_5 = N_1 e^{-\lambda \Delta t_5} \tag{9}$$

$$N_5 - N_1 = N_1 (e^{-\lambda \Delta t_5} - 1) \tag{10}$$

from eq. 1:

$$\Delta N_5 = N_1 (e^{-\lambda \Delta t_5} - 1) \tag{11}$$

therefore:

$$N_1 = \Delta N_5 / (e^{-\lambda \Delta t_5} - 1) \tag{12}$$

---

from eq. 8:

$$(Q - \lambda N_1) = (Q - \lambda N_5) e^{-\lambda \Delta t_1} \tag{13}$$

$$-\lambda N_1 = Q e^{-\lambda \Delta t_1} - Q - \lambda N_5 e^{-\lambda \Delta t_1} \tag{14}$$

$$-\lambda N_1 + \lambda N_5 = Q (e^{-\lambda \Delta t_1} - 1) - \lambda N_5 (e^{-\lambda \Delta t_1} - 1) \tag{15}$$

from eq. 2:

$$-\lambda \Delta N_1 = Q (e^{-\lambda \Delta t_1} - 1) - \lambda N_5 (e^{-\lambda \Delta t_1} - 1) \tag{16}$$

$$\lambda N_5 (e^{-\lambda \Delta t_1} - 1) = Q (e^{-\lambda \Delta t_1} - 1) + \lambda \Delta N_1 \tag{17}$$

$$N_5 = [(Q/\lambda)(e^{-\lambda \Delta t_1} - 1) + \Delta N_1] / (e^{-\lambda \Delta t_1} - 1) \tag{18}$$

$$N_5 = (Q/\lambda) + [\Delta N_1 / (e^{-\lambda \Delta t_1} - 1)] \tag{19}$$

---

from eqs. 3, 12 and 19: $\Delta N_5 = N_5 - N_1$

$$\Delta N_5 = (Q/\lambda) + [\Delta N_1 / (e^{-\lambda \Delta t_1} - 1)] - [\Delta N_5 / (e^{-\lambda \Delta t_5} - 1)] \tag{20}$$

from eq. 6:

$$Q = \lambda \{ \Delta N_5 + [\Delta N_5 / (e^{-\lambda \Delta t_1} - 1)] + [\Delta N_5 / (e^{-\lambda \Delta t_5} - 1)] \} \tag{21}$$

$$\Delta N_5 = (Q/\lambda) / \{ 1 + [1/(e^{-\lambda \Delta t_1} - 1)] + [1/(e^{-\lambda \Delta t_5} - 1)] \} \tag{22}$$

---

from eq. 7:

$$N_3 = N_1 e^{-\lambda \Delta t_3} \tag{23}$$

$$N_4 = N_1 e^{-\lambda (\Delta t_5 - \Delta t_4)} \tag{24}$$

from eq. 5 $$\Delta N_2 = N_1 (e^{-\lambda(\Delta t_5 - \Delta t_4)} - e^{-\lambda \Delta t_3}) \quad (25)$$

from eq. 12: $$\Delta N_2 = [\Delta N_5 / (e^{-\lambda \Delta t_5} - 1)][e^{-\lambda(\Delta t_5 - \Delta t_4)} - e^{-\lambda \Delta t_3}] \quad (26)$$

therefore; after substitution of equation 22 into equation 26, it follows that:

$$\Delta N_2 = \frac{(Q/\lambda)(e^{-\lambda(\Delta t_5 - \Delta t_4)} - e^{-\lambda \Delta t_3})}{(e^{-\lambda \Delta t_5} - 1)\{1 + [1/(e^{-\lambda \Delta t_1} - 1)] + [1/(e^{-\lambda \Delta t_5} - 1)]\}} \quad (27)$$

after further rearranging, equation 27 becomes:

$$\Delta N_2 = \frac{(Q/\lambda)(e^{\lambda(t-t_3)} - e^{\lambda(t_1+t_4)} - e^{\lambda(t_2+t_4)} + e^{\lambda t_4})}{(1 - e^{\lambda t})} \quad (28)$$

Defining N as the total number of alpha counts results in:

$$N = (\Delta N_2) T/t \quad (29)$$

$$N = \frac{TQ(e^{\lambda(t-t_3)} - e^{\lambda(t_1+t_4)} - e^{\lambda(t_2+t_4)} + e^{\lambda t_4})}{t\lambda(1 - e^{\lambda t})} \quad (29)$$

and from Meyerhof[2] the rate of ^{8}Li production (Q) is defined as:

$$Q = IN_0 A \sigma D / Z \epsilon M \quad (30)$$

where I, for this study, is:

$$I = (\#\ \text{of coul})(t)(t_1)/(t_2')^2 (T) \quad (31)$$

Therefore, substituting equations 30 and 31 into equation 29 yields:

$$N = \frac{AN_0 \sigma D (\#\ \text{of coul})(t_1)(e^{\lambda(t-t_3)} - e^{\lambda(t_1+t_4)} - e^{\lambda(t_2+t_4)} + e^{\lambda t_4})}{(t_2')^2 \lambda Z \epsilon M (1 - e^{\lambda t})} \quad (32)$$

Multipying equation 32 by the solid angle correction (Ω), dividing the total number of alpha counts (N) by 2 (correction for the isotropic decay of ^{8}Be) and solving for the cross section (σ) gives the cross section equation used in this study.

$$\sigma = \frac{\lambda(t_2')^2 NZ\epsilon M(1-e^{\lambda t})}{2\Omega N_0 A D t_1 (\#\ \text{of coul})(e^{\lambda(t-t_3)} - e^{\lambda(t_2+t_4)} - e^{\lambda(t_2+t_4)} + e^{\lambda t_4})} \quad (33)$$

EXPLANATION OF SYMBOLS IN CROSS SECTION DERIVATION

Symbol	Explanation
Q	Rate of ^{8}Li production from the $^{7}Li(d,p)^{8}Li$ reaction.
I	Beam current in coulombs.
Z	Charge/atom with respect to incident particles.
σ	Cross section for the $^{7}Li(d,p)^{8}Li$ reaction in cm^2. (1mb = $10^{-27} cm^2$)
ϵ	Number of coulombs/charge.
M	Atomic weight of target material in g/mole.
λ	Decay constant for the ^{8}Li beta decay.
A	Number of ^{7}Li atoms/molecule in target material.
D	Thickness of target in g/cm^2.
N_0	Avagadro's number (6.023×10^{23}).
t	Time/cycle within a run.
t_1	Time provided for irradiation of the target.
t_2'	Time provided for integration of the beam.
N	Total number of alpha counts/run.
T	Total time provided for a run.
Ω	Solid angle correction.

APPENDIX B

Energy Calibration of Accelerator

In order to provide an accurate energy scale for the $^{7}Li(d,p)^{8}Li$ excitation function determined in this study, the 2MeV Van de Graaff Accelerator used to determine this excitation function was energy calibrated using the 1.882MeV resonance from the $^{7}Li(p,n)^{7}Be$ reaction, the 0.770MeV and 1.02MeV resonances from the $^{7}Li(d,p)^{8}Li$ reaction, and the 0.837MeV resonance from the $^{19}F(p,\alpha\gamma)^{16}O$ reaction.

Using these resonances a plot of the magnet current corresponding to the energy values for these resonances versus the energy of the incident deuterons, calculated from the following equation:

$$E_d = E_p(M_p/M_d) \qquad (13)$$

for the $^{7}Li(p,n)^{7}Be$ and $^{19}F(p,\alpha\gamma)^{16}O$ reactions, was made. These points were fit using a least squares regression program[24] working through ten iterations. This least squares fit is shown in Figure 25 and indicates an energy calibration of this accelerator to within 1.5%.

As a result of this calibration the 0.770MeV and 1.02MeV resonances in the $^{7}Li(d,p)^{8}Li$ reaction appear at 0.777 ± 0.012MeV and 1.031 ± 0.015MeV respectively.

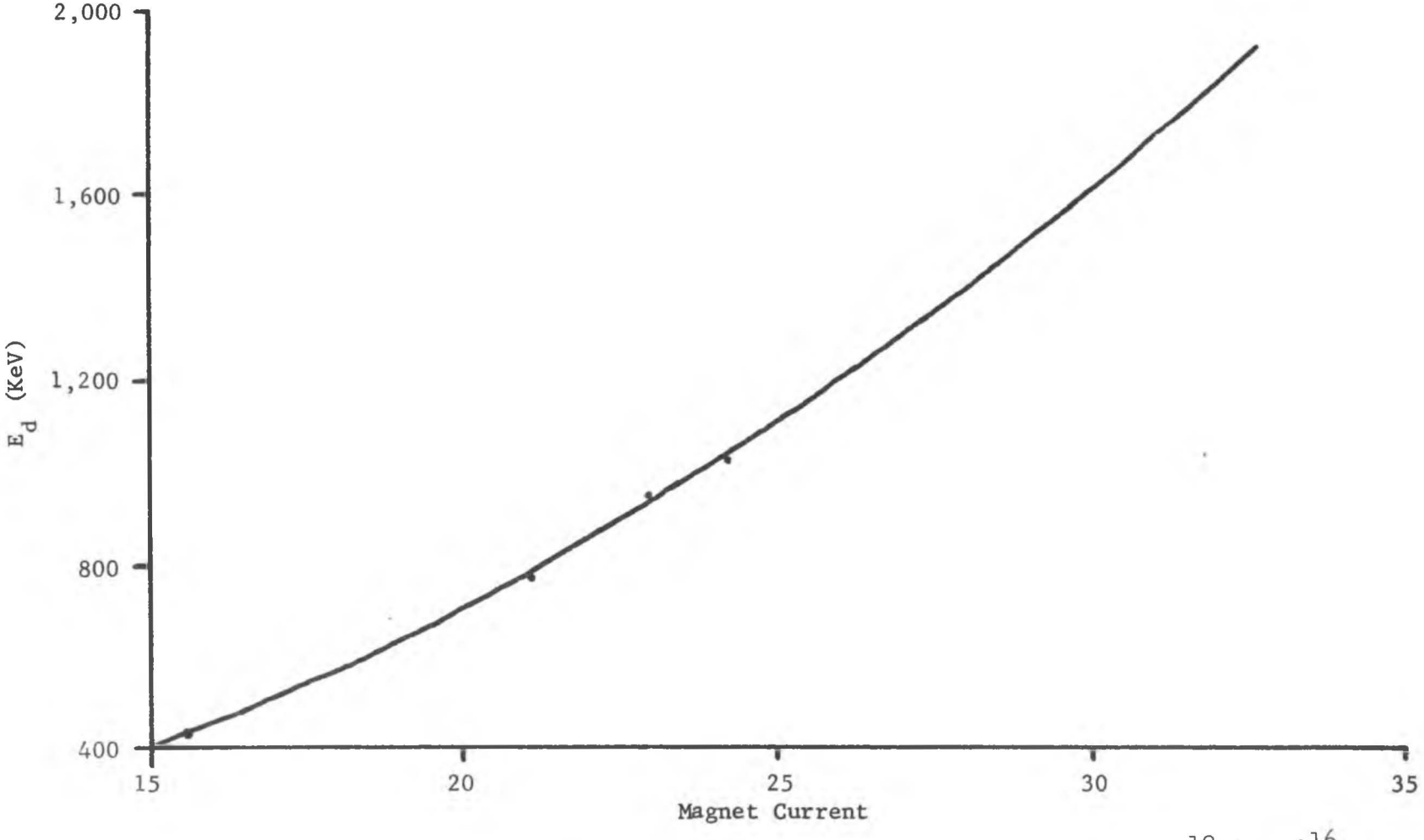

Fig. 25. Plot showing least squares fit to the 0.837MeV resonance from the $^{19}F(p,\alpha\gamma)^{16}O$ reaction, 0.770MeV resonance from the $^{7}Li(d,p)^{8}Li$ reaction, 1.882MeV resonance from the $^{7}Li(p,n)^{7}Be$ reaction, and 1.02MeV resonance from the $^{7}Li(d,p)^{8}Li$ reaction respectively.

APPENDIX C

DIGITAL PRINTOUT OF THE $^{7}Li(d,p)^{8}Li$ EXCITATION FUNCTION

The following is a listing of the cross section values and their corresponding energies for all 89 points on the $^{7}Li(d,p)^{8}Li$ excitation function shown in Figure 20. The uncertainity in these cross section values is listed; the uncertainity in the energy values, discussed in Appendix B, is $\pm 1.5\%$. These values are listed in the order in which they were experimentally obtained.

Energy (KeV)	Cross Section (mb)
623	66 ± 3
652	96 ± 4
668	115 ± 5
679	129 ± 5
689	141 ± 6
696	150 ± 6
713	169 ± 7
723	180 ± 8
731	184 ± 8
739	190 ± 8
748	195 ± 8
754	197 ± 8
762	200 ± 9

Energy (KeV)	Cross Section (mb)
769	201 ± 9
777	202 ± 9
786	200 ± 8
792	197 ± 8
800	195 ± 8
810	189 ± 8
821	187 ± 8
831	182 ± 8
852	176 ± 7
905	158 ± 7
920	155 ± 7
932	154 ± 7
944	154 ± 7
960	159 ± 7
978	164 ± 7
991	172 ± 7
1001	180 ± 8
1010	185 ± 8
1018	187 ± 8
1031	188 ± 8
1043	182 ± 8
1074	163 ± 7
1105	155 ± 7
1102	154 ± 7
1156	157 ± 7

Energy (KeV)	Cross Section (mb)
1243	172 ± 7
1342	189 ± 8
875	165 ± 7
1061	171 ± 7
1130	154 ± 7
1130	153 ± 7
1198	162 ± 7
1295	179 ± 8
1477	213 ± 9
1487	215 ± 9
1544	221 ± 9
1392	199 ± 8
933	154 ± 7
1128	153 ± 7
1223	167 ± 7
1274	176 ± 8
1347	188 ± 8
1372	195 ± 8
1383	196 ± 8
1389	200 ± 9
1394	200 ± 9
1397	201 ± 9
1399	202 ± 9
1402	202 ± 9
1410	202 ± 9
1416	204 ± 9

Energy (KeV)	Cross Section (mb)
1427	204±9
1437	207±9
1442	207±9
1450	209±9
1461	209±9
1466	211±9
1476	214±9
1481	213±9
1492	213±9
1503	216±9
1515	216±9
1613	230±10
1727	237±10
1516	219±9
1531	220±9
1558	227±10
1677	235±10
1728	240±10
1906	243±10
1128	154±7
1557	225±10
1669	236±10
1786	241±10
1847	242±10
1968	244±10

LIST OF REFERENCES

1. J. H. E. Mattauch, W. Thiele, and A. H. Wapstra, Nuc. Phys., 67, 1 (1965).

2. W. E. Meyerhof, Elements of Nuclear Physics (McGraw-Hill, Inc., New York, 1967), p. 171-223.

3. L. H. Rumbaugh, R. B. Roberts, and L. R. Hafstad, Phys. Rev., 54, 657 (1938).

4. W. E. Bennett, T. W. Bonner, H. T. Richards, and B. E. Watts, Phys. Rev., 71, 11 (1946).

5. L. M. Baggett and S. J. Bame, Jr., Phys. Rev., 85, 434 (1951).

6. S. Bashkin, Phys. Rev., 95, 1012 (1954).

7. L. S. Bezrukov, D. A. Panov, and D. V. Timoshuk, Sov. J. Nuc. Energy, 4, 609 (1956).

8. J. P. F. Sellschop, Phys. Rev., 119, 251 (1959).

9. R. W. Kavanagh, Nuc. Phys., 15, 411 (1960).

10. P. D. Parker, Phys. Rev., 150, 851 (1966).

11. D. H. Wilkinson, Proceedings of the International Conference on Nuclear Structure, Kingston, 1960 (North-Holland Publishing Co., Amsterdam, 1960), p. 42.

12. W. L. Imhof, L. F. Chase, and D. B. Fossan, Bull. Am. Phys. Soc., 9, 391 (1964).

13. J. B. Woods and D. H. Wilkinson, Nuc. Phys., 61, 661 (1965).

14. W. L. Imhof, L. F. Chase, and D. B. Fossan, Phys. Rev., 139, 904B (1965).

15. T. Lauritsen and F. Ajzenberg-Selove, Nuc. Phys., 78, 1 (1966).

16. D. H. Wilkinson and D. E. Alburger, Phys. Rev. Letts., 26, 1127 (1971).

17. H. Daniel, W. Collin, M. Kuntze, S. Margulies, B. Martin, O. Mehling, P. Schmidlin, and H. Schmitt, Nuc. Phys., A118, 689 (1968).

18. D. H. Claassen and H. Dinter, Nuc. Phys., 81, 155 (1966).

19. G. Dearnaley and D. C. Northrop, "Semiconductor Counters for Nuclear Radiations," E. and F. N. Spon Limited, London, England, 129 (1964).

20. P. G. Steward, "Stopping Power and Range for any Nucleus in the Specific Energy Interval 0.01-to-500MeV/amu in any Nongaseous Material," (Ph.D. dissertation, Dept. of Physics, Univ. of Calif. at Berkeley, 1968) pps. 1-100.

21. W. A. Fowler, C. C. Lauritsen, and T. Lauritsen, Revs. Mod. Phys., 20, 243 (1948).

22. C. F. Williamson, Jean-Paul Boujot, and J. Picard, Tables of Range and Stopping Power of Chemical Elements for Charged Particles of Energy 0.05 to 500MeV. (Report CEA-R 3042, Centre D'Etudes Nucleaires De Saclay, 1966), pps. 79 and 91).

23. K. Nielson, Brigham Young University, Private Communication, (1971).

24. K. P. Anderson and R. L. Snow, J. Chem. Ed., 44, 756, (1967).

$^{7}Li(d,p)^{8}Li$ EXCITATION FUNCTION:

E_d = 0.623MeV TO 1.968MeV

Albert E. Schilling

Department of Chemistry

M.S. Degree, April 1973

ABSTRACT

In this study the excitation function for the $^{7}Li(d,p)^{8}Li$ reaction is determined at incident deuteron energies ranging from 0.623MeV to 1.968MeV by counting the delayed alpha-particles as a result of the ^{8}Li beta decay. This excitation function reveals resonances at 0.777±0.012MeV and 1.031±0.015MeV with cross sections of 202±9mb and 188±8mb respectively.

The uncertainty in the cross section values was due to three independent sources of error within this experiment, the solid angle, the ^{8}Li half-life, and the target (LiF) thickness.

The uncertainty in the energy values was determined from an energy calibration of the accelerator used in this study. Resonances from the $^{7}Li(p,n)^{7}Be$ (1.882MeV), $^{7}Li(d,p)^{8}Li$ (0.770MeV; 1.02MeV) and $^{19}F(p,\alpha\gamma)^{16}O$ reactions were used in this energy calibration.